Research Square

Preprints are preliminary reports that have not undergone peer review.
They should not be considered conclusive, used to inform clinical practice,
or referenced by the media as validated information.

Deficiency of FRMD5 results in neurodevelopmental dysfunction and autistic-like behavior in mice

Yun Wang (wangy66@bjmu.edu.cn)
Peking University
Tian-Jie Lyu
Ji Ma
Xi-Yin Zhang
Guo-Guang Xie
Cheng Liu
Juan Du
Yi-Nuo Xu
De-Chao Yang
Cheng Cen
Peking University
Meng-Yuan Wang
Na-Yun Lyu
https://orcid.org/0000-0001-6554-2036
Hong-Quan Zhang

Article

Keywords:

Posted Date: August 7th, 2023

DOI: https://doi.org/10.21203/rs.3.rs-3202261/v1

License: This work is licensed under a Creative Commons Attribution 4.0 International License.
Read Full License

Additional Declarations: The authors have declared there is **NO** conflict of interest to disclose

Version of Record: A version of this preprint was published at Molecular Psychiatry on January 16th, 2024. See the published version at https://doi.org/10.1038/s41380-024-02407-w.

Title

Deficiency of FRMD5 results in neurodevelopmental dysfunction and autistic-like behavior in mice

Authors and affiliations

Tian-Jie Lyu[1, †], Ji Ma[2, †], Xi-Yin Zhang[1, †], Guo-Guang Xie [1, †], Cheng Liu[2, †], Juan Du[2, †], Yi-Nuo Xu[1], De-Cao Yang[2], Cheng Cen[1], Meng-Yuan Wang[2], Na-Yun Lyu[1], Yun Wang[1, 3, *], Hong-Quan Zhang[2, *]

1 Neuroscience Research Institute and Department of Neurobiology, School of Basic Medical Sciences, Key Laboratory for Neuroscience, Ministry of Education/National Health Commission, National Health Commission and State Key Laboratory of Natural and Biomimetic Drugs, Peking University, Beijing 100083, China

2 Department of Human Anatomy, Histology and Embryology, School of Basic Medical Sciences, State Key Laboratory of Molecular Oncology and International Cancer Institute, Peking University Health Science Center, Beijing 100083, China

3 PKU-IDG/McGovern Institute for Brain Research, Peking University, Beijing 100871, China

† These authors contributed equally

*Correspondence to: Hong-Quan Zhang (Hongquan.zhang@bjmu.edu.cn), Yun Wang (wangy66@bjmu.edu.cn).

Summary paragraph

Postsynaptic scaffolding proteins are causally associated with the pathophysiology of autism spectrum disorders (ASDs), a finding that is supported by several large-scale genomic studies [1,2] as well as *in vitro* and *in vivo* neurobiological studies of mutations in animal models [3,4]. However, since ASD patients illustrate distinct phenotypic and genetic heterogeneity, each individual mutation gene accounts for only a small proportion (<2%) of cases [1,5]. Recently, a human genetic study indicated that *de novo* variants in FERM domain-containing-5 (*FRMD5*) are related to neurodevelopmental abnormalities [6]. Here, we reveal that deficiency of the scaffolding protein FRMD5 results in neurodevelopmental dysfunction and ASD-like behavior in mice. FRMD5 deficiency leads to morphological abnormalities in neurons and synaptic dysfunction in mice. *Frmd5*-deficient mice exhibited learning and memory dysfunction, impaired social function, and increased repetitive stereotyped behavior. Mechanistically, tandem mass tag (TMT)-labeled quantitative proteomics showed that FRMD5 deletion affected the distribution of synaptic proteins involved in the pathological process of ASD. Taken together, our findings first delineate the critical role of FRMD5 in neurodevelopment and ASD pathophysiology, indicating a therapeutic potential for the treatment of ASD.

Main text

Introduction

Autistic spectrum disorder (ASD) is a group of neurodevelopmental diseases with social dysfunction, communication disorders, narrow interest and repetitive behavior as the core symptom onsets. As the diagnosis of autism has rapidly evolved over the past few decades, its prevalence is estimated to be 1-5% in developed countries [7,8]. The rising number of patients urges us to further elucidate the pathogenic mechanism of ASD. Recent research has revealed that ASD has multifactorial etiology and genetic heterogeneity that includes environmental, metabolic, immune, and genetic mechanisms as well as other risk factors [9,10]. A recent cohort analysis also found that the age of ASD patients ranges from 46 to 65 months, which indicates the crucial role of early neurodevelopment dysfunction in the course of ASD [11]. The pathogenic mechanism of ASD might be highly related to neurodevelopmental dysfunction in early development, and the symptoms will gradually worsen and expand during the whole period.

Although early pathogenic mechanisms might be corrected at an early timepoint to prevent phenotypic defects in adults, it is difficult to fully illustrate the innate mechanisms of neurodevelopmental dysfunction [12]. Among all the pathogenic models for ASD, SHANK3, a synaptic scaffolding protein that regulates the structural organization of dendritic spines, is highly associated with autistic spectrum disorder [13-15]. This demonstrates a strong urgency for the study of ASD-related synaptic structural proteins, which may help us to fully illustrate the pathophysiological mechanisms of ASD and identify more targets at the early timepoint for clinical medicine [16]. Surprisingly, we found that FRMD5, a novel

putative cytoskeletal protein [17], is highly associated with neurodevelopmental dysfunction. Further research on this gene revealed that FRMD5 deficiency could lead to ASD-like behavior in mice.

FRMD5 is a member of the FERM family of proteins that was first reported as a target gene regulated by p53 and was cloned in 2012. FRMD5 is located at the cell adherent junction, forms a molecular complex with p120-catenin through its C-terminal region, may play a role in p120-catenin-based cell–cell contact and is involved in the regulation of tumor progression [17,18]. Recently, a human genetic study reported that *de novo* variants in *FRMD5* are related to neurodevelopmental abnormalities in humans [6]. Three interactive web-based databases (DECIPHER [19], ClinVar, and GeneMatcher [20,21]) recording genotype-phenotype correlations have collected 4 ASD patients and 6 patients with varying degrees of neurodevelopment abnormalities, all of whom share a common feature of either having a single nucleotide missense mutation in *FRMD5* or a large segmental deletion spanning the *FRMD5* gene (**Table S1**). This evidence suggests that genetic variations affecting the *FRMD5* gene may play a role in the development of ASD.

To elucidate the potential involvement of *FRMD5* in the pathological process, this study utilized a comprehensive array of techniques and methods in the fields of biochemistry, molecular biology, behavior, morphology, electrophysiology, and proteomics. With *Frmd5* knockout mice, we found that deficiency of the scaffolding protein FRMD5 results in neurodevelopmental dysfunction and ASD-like behavior. Comparisons between our study and other rodent models of ASD show the urgent need to understand the heterogeneity in ASD to offer potential drug targets of ASD on FRMD5.

Results

FRMD5 is highly expressed in the nervous system, especially at the early stage of brain development in mice

The expression pattern of *Frmd5* was verified through RT–qPCR analysis of RNA from various organs in mice (Fig. 1A), demonstrating a similarity to the pattern observed in humans (Fig. S1A-S1B). Western blot analysis of the cortex and hippocampus across stages in brain development also showed that FRMD5 is highly expressed at the early stage of brain development in mice, especially at E18.5 (Fig. 1B). To further illustrate the function of FRMD5, we created *Frmd5*-KO mice by specifically deleting one or two bases in the 6^{th} exon (Fig. S1C-S1E).

Knockout of *Frmd5* leads to ASD-like behavioral abnormalities in mice

Autism spectrum disorder leads to deficits in social-emotional reciprocity and restricted, repetitive patterns of behavior [7]. To reveal the potential function of *Frmd5* in ASD, we applied a three-chambered social approach task and compulsive behavior tests. Using the three-chambered social approach task, we found that knockout of *Frmd5* led to a lower preference index in the short-term social memory task between 2 stranger positions than in the social preference task between strangers and objects (Fig. 1C-1G). Notably, by olfactory habituation/discrimination experiments, knockout of *Frmd5* did not affect olfactory sensation in mice (Fig. S2A-S2B); thus, we can attribute the social abnormalities to the deficiency of social memory. We also observed more compulsive behaviors in *Frmd5*-KO mice, including grooming, climbing and jumping (Fig. 1H-1L).

In clinical practice, ASD patients also suffer from memory abnormalities [7]; thus, we

applied more memory tests to measure memory abnormalities in *Frmd5*-KO mice. Before the memory tests, we used the rotarod test and pup mouse ultrasonic vocalization test to ensure the memory of *Frmd5*-KO mice. We found that knockout of *Frmd5* did not affect motor or audiometric functions (Fig. S2C-S2G). Then, we found that *Frmd5*-KO mice showed a deficiency in novel object and place/position recognition in the novel object and place/position recognition test (Fig. 1M-1R). In terms of spatial memory, *Frmd5* KO in mice affected spatial memory in the Y maze (Fig. 1S-1U) but not in the Morris water maze or spatial working memory in the Y maze (Fig. S2H-S2L). Moreover, anxiety and nociception did not show significant changes in *Frmd5*$^{-/-}$ mice in the open field test, elevated O-maze, hot plate test or von Frey test (Fig. S2M-S2V). Overall, knockout of *Frmd5* led to complex ASD-like behavioral abnormalities in mice, including social deficiency, increased compulsive behaviors and memory abnormalities (Table S2-S4).

Knockout of *Frmd5* leads to abnormal dendritic branching and spine morphology in the hippocampus

To further investigate the innate function of FRMD5 in the nervous system, we identified its distribution in various brain regions. The Western blot results showed that FRMD5 is highly expressed in the hippocampus, especially in the CA1 and DG (Fig. S3A). Recent research has indicated that neuronal dendrite synaptogenesis developmental abnormalities are pathological factors in ASD [4,22]. Knockout of *Frmd5* led to a decrease in the length and complexity of basal dendrites on CA1 pyramidal neurons (Fig. 2A-2B) but did not affect the length or complexity of apical dendrites on CA1 pyramidal neurons visualized by Golgi-Cox staining (Fig. 2C). Notably, by sparse neuron labeling in the DG, we found that

Frmd5-KO did not affect the length or complexity of dendrites (Fig. 2D), although it led to an increase in stubby dendrite spines (Fig. 2E-2G). Moreover, knockout of *Frmd5* led to longer heads and lengths of mushroom and long/thin spines, which showed more immature spines in *Frmd5*-KO mice (Fig. 2H) but did not affect the migration of mouse cortical neurons *in vivo* or the polarity of primary cultured hippocampal neurons (Fig. S3B-S3K). Taken together, deficiency of FRMD5 leads to neurodevelopmental dysfunction by abnormal dendritic branching and spine morphology.

Knockout of *Frmd5* leads to increased intrinsic excitability and decreased neuronal transmission in granule cells of the DG

To examine the potential impact of previously identified morphological alterations in neurons on synaptic transmission function, we applied the whole-cell patch-clamp technique to DG granule cells of *Frmd5*-KO mice. The results showed that FRMD5 deficiency led to increased input resistance, which revealed increased intrinsic excitability in granule cells of the DG (Fig. 3A-3C). After current injection from a baseline potential, a lower injected current led to an increased number of spines in $Frmd5^{-/-}$ DG granule cells (Fig. 3D-3E); however, a higher injected current led to decreased responsivity (Fig. 3F). Moreover, the frequency of spontaneous excitatory postsynaptic currents (sEPSCs) decreased in $Frmd5^{-/-}$ DG granule cells, which led to a decrease in neuronal transmission to DG neurons (Fig. 3G-3I). Furthermore, the injected current that induced the first 5 Hz action potential showed that knockout of *Frmd5* does not affect the threshold or amplitude of DG neurons (Fig. 3J-3L).

Synaptosomes of *Frmd5*$^{-/-}$ mice reveal that FRMD5 is highly related to ASD risk gene-coded proteins

To investigate the molecular mechanism underlying the abnormal function and behavior of mouse neurons caused by the deletion of *Frmd5*, we examined the subcellular localization of the FRMD5 protein in neurons using live cell imaging and synaptic component isolation. First, with live cell imaging of primary hippocampal neurons, we found that FRMD5 is located at the cell membrane and cell-matrix adhesion, especially at the dendritic shaft, branch point and basilar region of the dendritic spine (Fig. S4, supplementary video S1 and S2). Second, we separated cell components by gradient sucrose centrifugation for Western blotting. The results showed that FRMD5 was mainly distributed in the cytoplasm and internal membrane structures, especially in the postsynaptic density (PSD) component (Fig. 4A). Finally, we performed tandem mass tag (TMT)-labeled quantitative proteomics to gain insight into the wider effects of FRMD5 deficiency on the cellular proteome and the underlying molecular mechanism, by which we found that FRMD5 is highly associated with ASD risk gene-coded proteins, including SHANK3, CEP290, CAMK2A and CAMK2B (Fig. 4B-4C). Gene Ontology (GO) analysis revealed that FRMD5 deficiency is highly related to synapse and neurotransmitter receptors, especially the activation of synaptic AMPA and NMDA receptors and their neurotransmission (Fig. 4D-4E). Furthermore, Western blot analysis verified that FRMD5 deficiency leads to reduced expression of the SHANK3 and CAMK family scaffolding proteins, which shows a potential correlation between SHANK3 and FRMD5 in ASD (Fig. 4F-4H).

Discussion

Autistic spectrum disorder is a group of complex symptoms [8] whose high prevalence worldwide urges us to further illustrate the innate pathological processes driving this disease. Although a previous twin study showed great heredity in symptoms among ASD patients, there are still differences in specific symptoms, such as cognitive level and related symptoms. Therefore, phenotypic heterogeneity has become the basic research point of ASD [7]. With the advantages of improvements in gene screening and whole exome sequencing (WES), researchers can further illustrate the pathological process under phenotypic heterogeneity. Among the highlights of these studies, some scaffolding proteins found by sequencing show innate effects on ASD developmental dysfunction [13,14]. Scaffolding proteins are usually the core components of biological processes. Recent research on SHANK3, a scaffolding protein, inspired us to further concentrate on other ASD-related scaffolding proteins.

By searching the database of clinical and genetic information, we found that four ASD patients and six neurodevelopmental disorder patients carried *FRMD5* deletions/mutations [19-21]. Recent research has also indicated that *de novo FRMD5* can lead to neurodevelopmental abnormalities in humans [6]. On the other hand, ASD is highly related to dysfunction at the early stage of neurodevelopment, and we surprisingly found that FRMD5 is also highly expressed in the nervous system, especially at the early stage of brain development in mice. To further illustrate the function of FRMD5, we generated *Frmd5*-KO mice. Behavioral experiments showed that knockout of *Frmd5* leads to ASD-like behavioral abnormalities in mice. *Frmd5*-KO mice show classical ASD-like

behavioral abnormalities, but some symptoms, such as nociceptive abnormalities, are not present in *Frmd5*-KO mice. These results show that FRMD5 is not the only gene related to ASD, and more research is needed on the multifactorial etiology of ASD.

Recent research has revealed that ASD is related to several neurobiological abnormalities, including changes in cortical structure and connectivity, morphological abnormalities of neurons, abnormal synaptogenesis, and synaptic dysfunction [23-25]. We found that knockout of *Frmd5* can lead to abnormal dendritic branching and spine morphology in the hippocampus and increased intrinsic excitability in granule cells of the DG in mice. Along with the analysis of synaptosomes, our results revealed a mechanism of neuronal structural abnormalities in the pathological process of autism, which is related to the dysfunction of glutamatergic synapses in autism patients [26]. Notably, other murine studies also found that changes in synaptic transmission and plasticity beyond the normal range, whether increased or decreased, lead to social disorder [27]. According to our study, longer head and length of mushroom and long/thin spines show potential immaturity and abnormalities in spine pruning of ASD at the early stage. Taken together, FRMD5 may play an important role in neurodevelopmental deficiency in ASD.

ASD is considered to be caused by abnormal global brain remodeling in the early developmental stage. Recent neuroimaging studies have proven the pattern of excessive brain volume growth in infants and young children with ASD [28]. Compared with children in normal development, children with ASD experience accelerated brain development at an early stage, resulting in connectivity changes [29], including insufficient connectivity of the whole brain and over-connectivity in specific areas, especially the frontal lobe and

occipital bone area [30]. In our study, although the dendrite growth and synapse of *Frmd5*-KO mice were involved, immunohistochemistry and brain morphology analyses showed no specific changes in the brain structure or cell composition of KO mice (Fig. S3 and Table S2-S4), indicating that FRMD5 is involved in the regulation of the innate nervous system mechanism.

Synaptosomes of *Frmd5*-KO mice also revealed that *Frmd5* is highly related to ASD risk genes. According to the results of TMT-labeled quantitative proteomics experiments, we found that knockout of *Frmd5* leads to changes in Ca^{2+}/CaM-dependent family protein kinases, glutamate type *N*-methyl-D-aspartate (NMDA) receptor subunits and other ASD-related proteins. Among these proteins, CEP290, a centrosome and ciliary protein, showed higher expression in *Frmd5*-KO mice. Notably, recent research has found that mutations in *CEP290* are associated with intellectual disability [31]. Moreover, knockout of *Frmd5* also leads to lower expression of SHANK1 and SHANK3. To further illustrate the innate pathological process of ASD, it is important to reveal the interaction between *Frmd5* and these ASD-related proteins.

At the cellular level, FRMD5 protein deficiency results in abnormal neuronal morphology and altered dendritic spine density. At the functional level, it causes a decrease in excitatory input and an increase in the intrinsic excitability of neurons. While this study did not delve deeply into this matter, our proteomic analysis revealed altered levels of multiple glutamatergic ionotropic NMDA receptor subtypes at synaptic sites. Future research may further investigate whether FRMD5 directly binds to NR2A and NR2B or even modulates the supramembrane processes of NMDARs. Additionally, investigating whether the use of

specific NMDA receptor agonists or inhibitors can partially restore ASD-like neurological function and behavioral phenotypes is another avenue for further exploration.

To our knowledge, there are few studies on the functions of the FERM domain-containing protein superfamily in the nervous system. This study represents the pioneering work that comprehensively explores the involvement of the FRMD5 protein in the molecular, morphological, synaptic, and behavioral aspects of neural development and ASD pathology, shedding new light on the role of FERM domain-containing proteins in the nervous system. The generation of Frmd5 whole-body knockout mice has provided valuable insight into the intricate functions and mechanisms of action of the FERM domain-containing protein superfamily in the nervous system. This study thus serves as a significant reference for future research exploring the functions of this protein family member in the nervous system.

Above all, our findings provide new insights into the personalized and precise treatment of ASD patients, and more research on its innate mechanism and potential value for clinical practice is still needed.

References

1 de la Torre-Ubieta, L., Won, H., Stein, J. L. & Geschwind, D. H. Advancing the understanding of autism disease mechanisms through genetics. *Nat Med* **22**, 345-361, doi:10.1038/nm.4071 (2016).

2 Bourgeron, T. From the genetic architecture to synaptic plasticity in autism spectrum disorder. *Nat Rev Neurosci* **16**, 551-563, doi:10.1038/nrn3992 (2015).

3 Huguet, G., Benabou, M. & Bourgeron, T. in *A Time for Metabolism and Hormones* (eds P. Sassone-Corsi & Y. Christen) 101-129 (2016).

4 Monteiro, P. & Feng, G. SHANK proteins: roles at the synapse and in autism spectrum disorder. *Nat Rev Neurosci* **18**, 147-157, doi:10.1038/nrn.2016.183 (2017).

5 Huguet, G., Benabou, M. & Bourgeron, T. in *A Time for Metabolism and Hormones* (eds P. Sassone-Corsi & Y. Christen) 101-129 (2016).

6 Lu, S. *et al.* De novo variants in FRMD5 are associated with developmental delay, intellectual disability, ataxia, and abnormalities of eye movement. *Am J Hum Genet* **109**, 1932-1943, doi:10.1016/j.ajhg.2022.09.005 (2022).

7 Lord, C., Elsabbagh, M., Baird, G. & Veenstra-Vanderweele, J. Autism spectrum disorder. *Lancet (London, England)* **392**, 508-520, doi:10.1016/S0140-6736(18)31129-2 (2018).

8 Lord, C. & Bishop, S. L. Recent advances in autism research as reflected in DSM-5 criteria for autism spectrum disorder. *Annu Rev Clin Psychol* **11**, 53-70, doi:10.1146/annurev-clinpsy-032814-112745 (2015).

9 Baribeau, D. & Anagnostou, E. Novel treatments for autism spectrum disorder based on genomics and systems biology. *Pharmacol Ther* **230**, 107939, doi:10.1016/j.pharmthera.2021.107939 (2022).

10 Jiang, C.-C. *et al.* Signalling pathways in autism spectrum disorder: mechanisms and therapeutic implications. *Signal Transduct Target Ther* **7**, 229, doi:10.1038/s41392-022-01081-0 (2022).

11 Shaw, K. A. *et al.* Progress and Disparities in Early Identification of Autism Spectrum Disorder: Autism and Developmental Disabilities Monitoring Network, 2002-2016. *J Am Acad Child Adolesc Psychiatry* **61**, 905-914, doi:10.1016/j.jaac.2021.11.019 (2022).

12 Chung, C., Shin, W. & Kim, E. Early and Late Corrections in Mouse Models of Autism Spectrum Disorder. *Biological Psychiatry* **91**, 934-944, doi:10.1016/j.biopsych.2021.07.021 (2022).

13 Durand, C. M. *et al.* Mutations in the gene encoding the synaptic scaffolding protein SHANK3 are associated with autism spectrum disorders. *Nature Genetics* **39**, 25-27 (2007).

14 Shcheglovitov, A. *et al.* SHANK3 and IGF1 restore synaptic deficits in neurons from 22q13 deletion syndrome patients. *Nature* **503**, 267-271, doi:10.1038/nature12618 (2013).

15 Tatavarty, V. *et al.* Autism-Associated Shank3 Is Essential for Homeostatic Compensation in Rodent V1. *Neuron* **106**, doi:10.1016/j.neuron.2020.02.033 (2020).

16 Bourgeron, T. From the genetic architecture to synaptic plasticity in autism spectrum disorder. *Nature Reviews. Neuroscience* **16**, 551-563, doi:10.1038/nrn3992 (2015).

17 Wang, T. *et al.* FERM-containing protein FRMD5 is a p120-catenin interacting protein that regulates tumor progression. *FEBS Letters* **586**, 3044-3050, doi:10.1016/j.febslet.2012.07.019 (2012).

18 Brázdová, M. *et al.* Modulation of gene expression in U251 glioblastoma cells by binding of

mutant p53 R273H to intronic and intergenic sequences. *Nucleic Acids Research* **37**, 1486-1500, doi:10.1093/nar/gkn1085 (2009).

19 Firth, H. V. *et al.* DECIPHER: Database of chromosomal imbalance and phenotype in humans using ensembl resources. *Am J Hum Genet* **84**, 524-533, doi:10.1016/j.ajhg.2009.03.010 (2009).

20 Sobreira, N., Schiettecatte, F., Valle, D. & Hamosh, A. GeneMatcher: a matching tool for connecting investigators with an interest in the same gene. *Hum Mutat* **36**, 928-930, doi:10.1002/humu.22844 (2015).

21 Sobreira, N., Schiettecatte, F., Boehm, C., Valle, D. & Hamosh, A. New tools for Mendelian disease gene identification: PhenoDB variant analysis module; and GeneMatcher, a web-based tool for linking investigators with an interest in the same gene. *Hum Mutat* **36**, 425-431, doi:10.1002/humu.22769 (2015).

22 Lin, Y. C., Frei, J. A., Kilander, M. B., Shen, W. & Blatt, G. J. A Subset of Autism-Associated Genes Regulate the Structural Stability of Neurons. *Front Cell Neurosci* **10**, 263, doi:10.3389/fncel.2016.00263 (2016).

23 Iakoucheva, L. M., Muotri, A. R. & Sebat, J. Getting to the Cores of Autism. *Cell* **178**, 1287-1298, doi:10.1016/j.cell.2019.07.037 (2019).

24 Quesnel-Vallières, M., Weatheritt, R. J., Cordes, S. P. & Blencowe, B. J. Autism spectrum disorder: insights into convergent mechanisms from transcriptomics. *Nat Rev Genet* **20**, 51-63, doi:10.1038/s41576-018-0066-2 (2019).

25 Mullins, C., Fishell, G. & Tsien, R. W. Unifying Views of Autism Spectrum Disorders: A Consideration of Autoregulatory Feedback Loops. *Neuron* **89**, 1131-1156, doi:10.1016/j.neuron.2016.02.017 (2016).

26 Moretto, E., Murru, L., Martano, G., Sassone, J. & Passafaro, M. Glutamatergic synapses in neurodevelopmental disorders. *Prog Neuropsychopharmacol Biol Psychiatry* **84**, 328-342, doi:10.1016/j.pnpbp.2017.09.014 (2018).

27 Lee, E., Lee, J. & Kim, E. Excitation/Inhibition Imbalance in Animal Models of Autism Spectrum Disorders. *Biol Psychiatry* **81**, 838-847, doi:10.1016/j.biopsych.2016.05.011 (2017).

28 Ecker, C., Bookheimer, S. Y. & Murphy, D. G. Neuroimaging in autism spectrum disorder: brain structure and function across the lifespan. *The Lancet. Neurology* **14**, 1121-1134, doi:10.1016/s1474-4422(15)00050-2 (2015).

29 Lewis, J. D. *et al.* Network inefficiencies in autism spectrum disorder at 24 months. *Transl Psychiatry* **4**, e388, doi:10.1038/tp.2014.24 (2014).

30 O'Reilly, C., Lewis, J. D. & Elsabbagh, M. Is functional brain connectivity atypical in autism? A systematic review of EEG and MEG studies. *PLoS One* **12**, e0175870, doi:10.1371/journal.pone.0175870 (2017).

31 Khoshbakht, S. *et al.* CEP104 and CEP290; Genes with Ciliary Functions Cause Intellectual Disability in Multiple Families. *Arch Iran Med* **24**, 364-373, doi:10.34172/aim.2021.53 (2021).

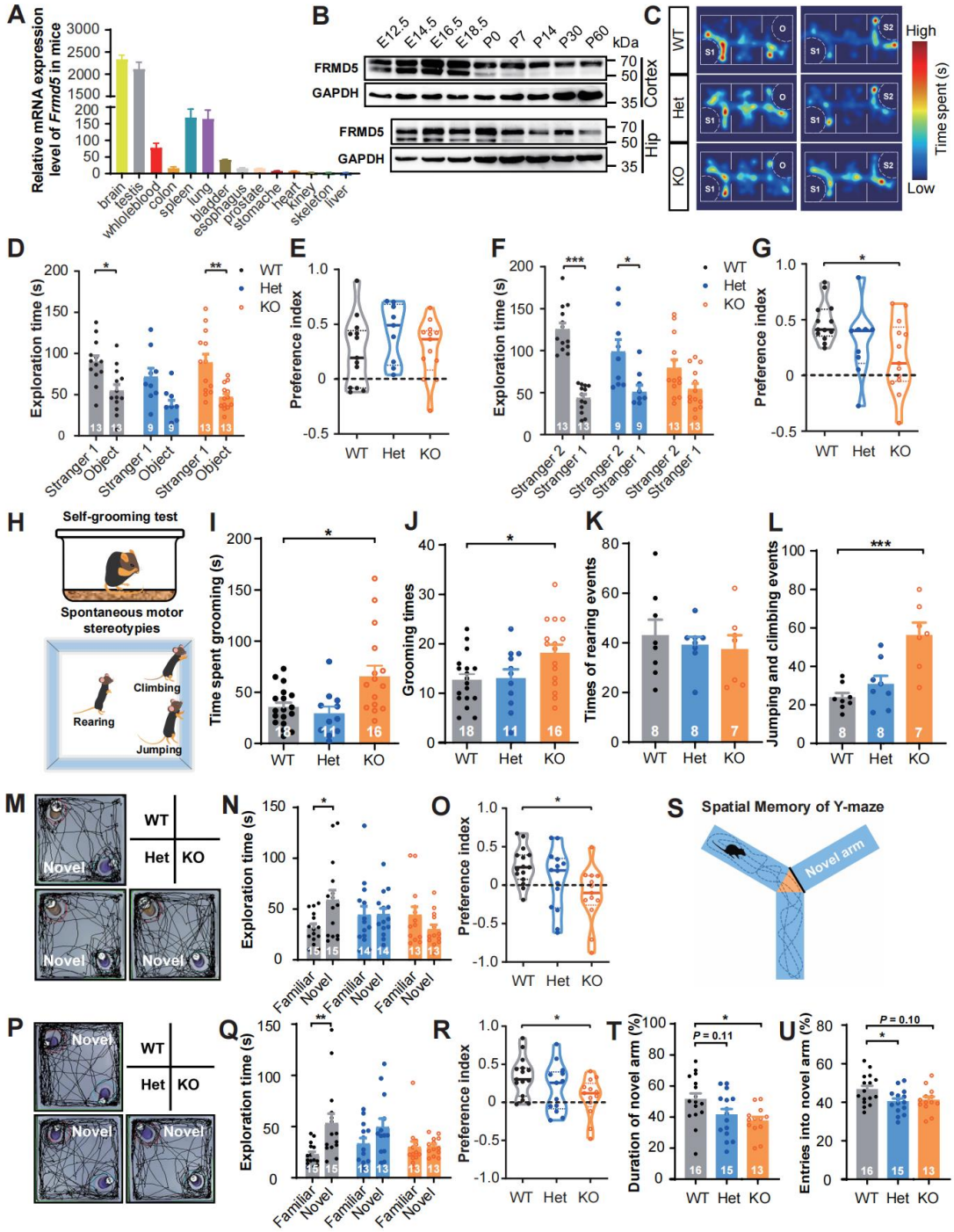
A
Relative mRNA expression level of Frmd5 in mice
brain
testis
wholeblood
colon
spleen
lung
bladder
esophagus
prostate
stomache
heart
kiney
skeleton
liver
B
E12.5
E14.5
E16.5
E18.5
P0
P7
P14
P30
P60
kDa
FRMD5
GAPDH
Cortex
Hip
C
WT
Het
KO
High
Low
Time spent (s)
D
Exploration time (s)
Stranger 1
Object
E
Preference index
F
Stranger 2
Stranger 1
G
H
Self-grooming test
Spontaneous motor stereotypies
Climbing
Rearing
Jumping
I
Time spent grooming (s)
J
Grooming times
K
Times of rearing events
L
Jumping and climbing events
M
Novel
N
Familiar
Novel
O
S
Spatial Memory of Y-maze
Novel arm
P
Q
R
T
Duration of novel arm (%)
P = 0.11
U
Entries into novel arm (%)
P = 0.10

332

333

Figure 1. Knockout of *Frmd5* leads to ASD-like behavioral abnormalities in mice.

(**A**) Relative mRNA expression of *Frmd5* in various organs and tissues of mice. (**B**) Expression of FRMD5 in the mouse cortex and hippocampus across developmental stages. The peak expression in the cortex is on E18.5, and that in the hippocampus is on P0. (**C-G**) *Frmd5*$^{-/-}$ mice exhibit impaired social ability. (C) Heatmap of the exploration time at different positions in 5 minutes. (D and E) Exploration time and preference index of the social preference task between stranger and object in 5 minutes. (F and G) Exploration time and preference index of the social memory task between 2 stranger positions in 5 minutes. (**H-L**) *Frmd5*$^{-/-}$ mice exhibit increased compulsive behaviors. (H) Schematic diagram of the self-grooming test and spontaneous motor behaviors in the open field test. (I) Time spent in the self-grooming test. Times of grooming events (J), rearing events (K), and jumping and climbing events (L) in the open field test. (**M-R**) *Frmd5*$^{-/-}$ mice exhibited impaired recognition ability in the novel object and novel place/position recognition tests. (M) Trace diagram of novel object recognition. (N and O) Exploration time and preference index of novel object recognition. (P) Trace diagram of novel position recognition. (Q and R) Exploration time and preference index of novel position recognition. (**S-U**) *Frmd5*$^{-/-}$ mice exhibit impaired spatial memory in the Y-maze test. (S) Schematic diagram of the spatial memory test in the Y-maze. (T-U) Duration of novel arm and entries into novel arm in the Y-maze.

Data are represented as the means ± SEM. Unpaired t test in (D), (F), (N) and (Q); one-way ANOVA with Tukey's multiple comparisons test in (E), (G), (I-L), (O), (R), (T) and

356 (U). *$P < 0.05$, **$P < 0.01$, ***$P < 0.001$.

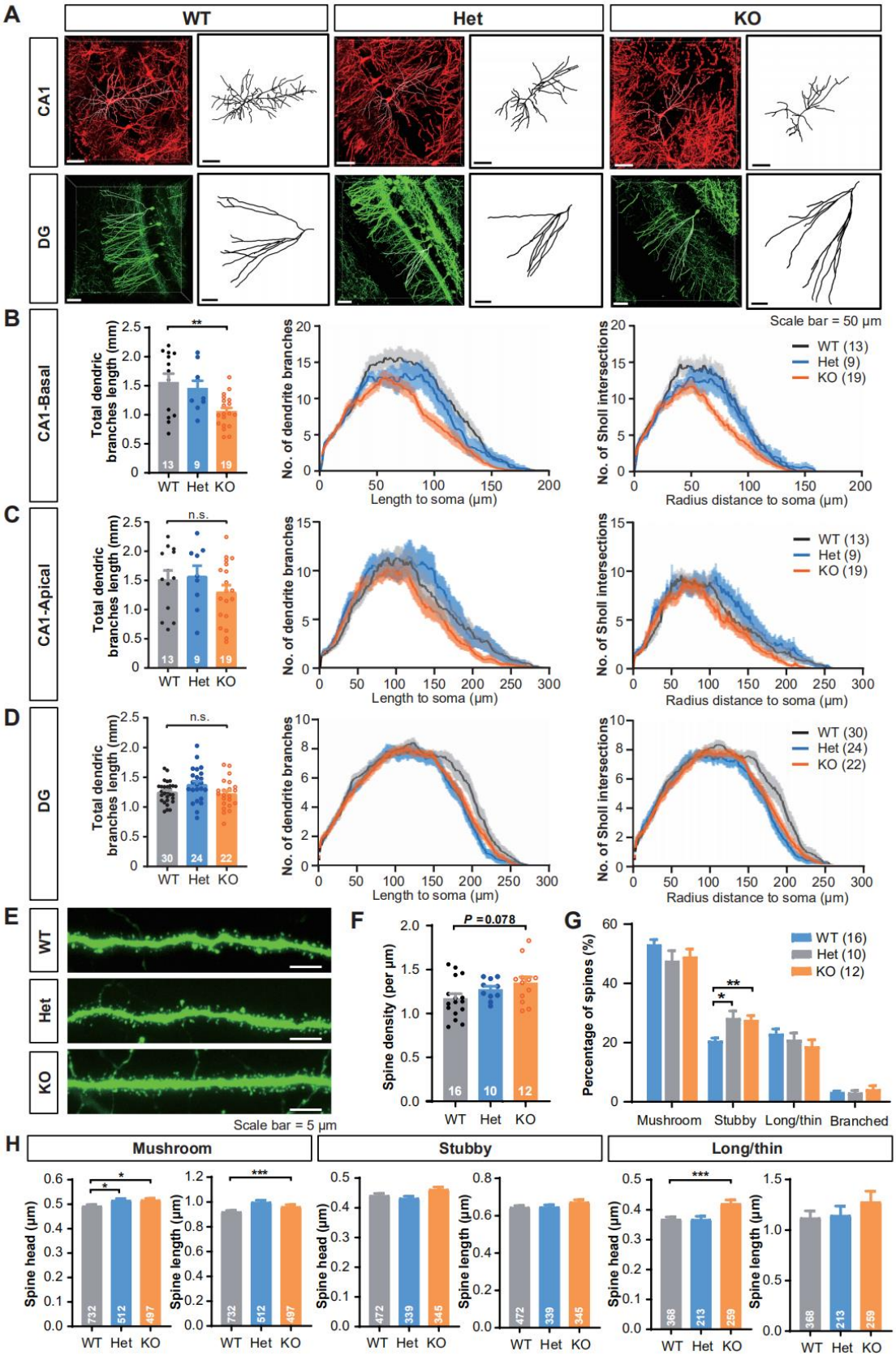
A
WT
Het
KO
CA1
DG
B
CA1-Basal
Total dendric branches length (mm)
No. of dendrite branches
Length to soma (μm)
No. of Sholl intersections
Radius distance to soma (μm)
Scale bar = 50 μm
WT (13)
Het (9)
KO (19)
C
CA1-Apical
n.s.
D
DG
WT (30)
Het (24)
KO (22)
E
Scale bar = 5 μm
F
P = 0.078
Spine density (per μm)
G
Percentage of spines (%)
WT (16)
Het (10)
KO (12)
Mushroom
Stubby
Long/thin
Branched
H
Spine head (μm)
Spine length (μm)

Figure 2. Knockout of *Frmd5* leads to abnormal dendritic branching in the basal CA1 region and abnormal spine morphology.

(**A**) Diagram of Golgi-Cox staining in CA1 and sparse labeling of GFP in DG. Scale bar = 50 μm. (**B**-**D**) *Frmd5*$^{-/-}$ mice exhibit abnormal dendritic branching in CA1-basal dendrites. (B) Total dendritic branch length (left), dendrite branches growing outward with dendrite length (middle), and Sholl intersections with varying radial circles (right) of CA1-basal dendrites in the hippocampus. (C) Total dendritic branch length, number of dendrite branches and Sholl intersections of CA1-apical dendrites in the hippocampus. (D) Total dendric branch length (left), dendrite branches growing outward with dendrite length (middle), and Sholl intersections with varying radial circles (right) of the DG in the hippocampus. (**E**) Diagram of dendritic spines in the DG with sparse labeling of GFP. Scale bar = 5 μm. (**F**) Spine density of the DG in the hippocampus. (**G**) Percentage of spines in the DG. (**H**) Head and length of mushroom (left), stubby (middle) and long/thin (right) spines.

Data are represented as the means ± SEM. One-way ANOVA with Tukey's multiple comparisons test in (B-D & F-H). *$P < 0.05$, **$P < 0.01$, ***$P < 0.001$. n.s., no significant difference.

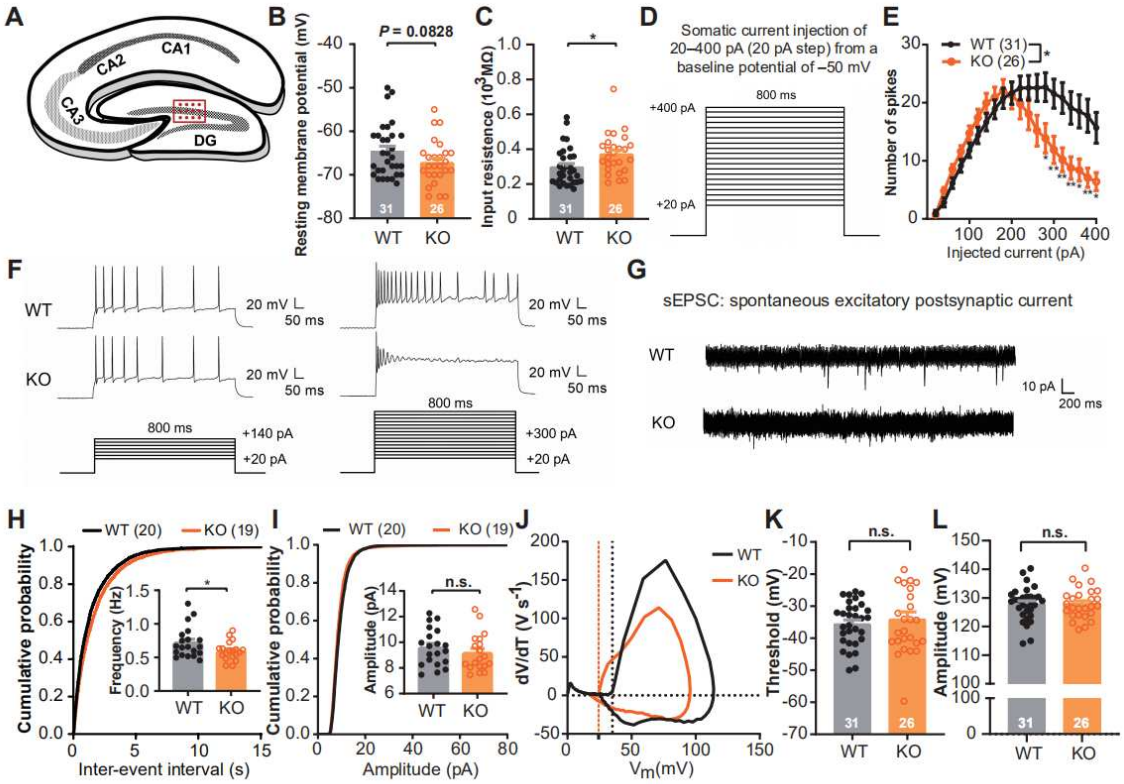
A
CA1
CA2
CA3
DG
B
P = 0.0828
Resting membrane potential (mV)
WT
KO
C
Input resistence (10^3MΩ)
D
Somatic current injection of 20–400 pA (20 pA step) from a baseline potential of –50 mV
800 ms
+400 pA
+20 pA
E
WT (31)
KO (26)
Number of spikes
Injected current (pA)
F
20 mV
50 ms
800 ms
+140 pA
+20 pA
+300 pA
G
sEPSC: spontaneous excitatory postsynaptic current
10 pA
200 ms
H
WT (20)
KO (19)
Cumulative probability
Inter-event interval (s)
Frequency (Hz)
I
Amplitude (pA)
n.s.
J
dV/dT (V s^-1)
Vm(mV)
K
Threshold (mV)
L
Amplitude (mV)

377

378

Figure 3. Knockout of *Frmd5* leads to increased intrinsic excitability in granule cells of the DG.

(**A**) Schematic diagram of patch clamp electrophysiology; the red box indicates the record position. (**B**) Resting membrane potential of DG neurons. (**C**) Input resistance of DG neurons. (**D**) Schematic diagram of passive excitatory recording on DG neurons. (**E**) Number of spikes of DG neurons. (**F**) Schematic diagram of action potential spikes with injected current (140 pA and 300 pA). (**G**) Schematic diagram of the spontaneous excitatory postsynaptic current of DG neurons. (**H** and **I**) Cumulative probability of the frequency and amplitude of sEPSCs. (**J**) Derivative analysis graph of the first 5 Hz action potential induced by DG neurons. (**K** and **L**) Depolarization threshold and amplitude of the first 5 Hz action potential.

Data are represented as the means ± SEM. Unpaired t test in (B), (C), (H), (I), (K) and (L); two-way ANOVA with Tukey's multiple comparisons test in (E). *$P < 0.05$, n.s., no significant difference.

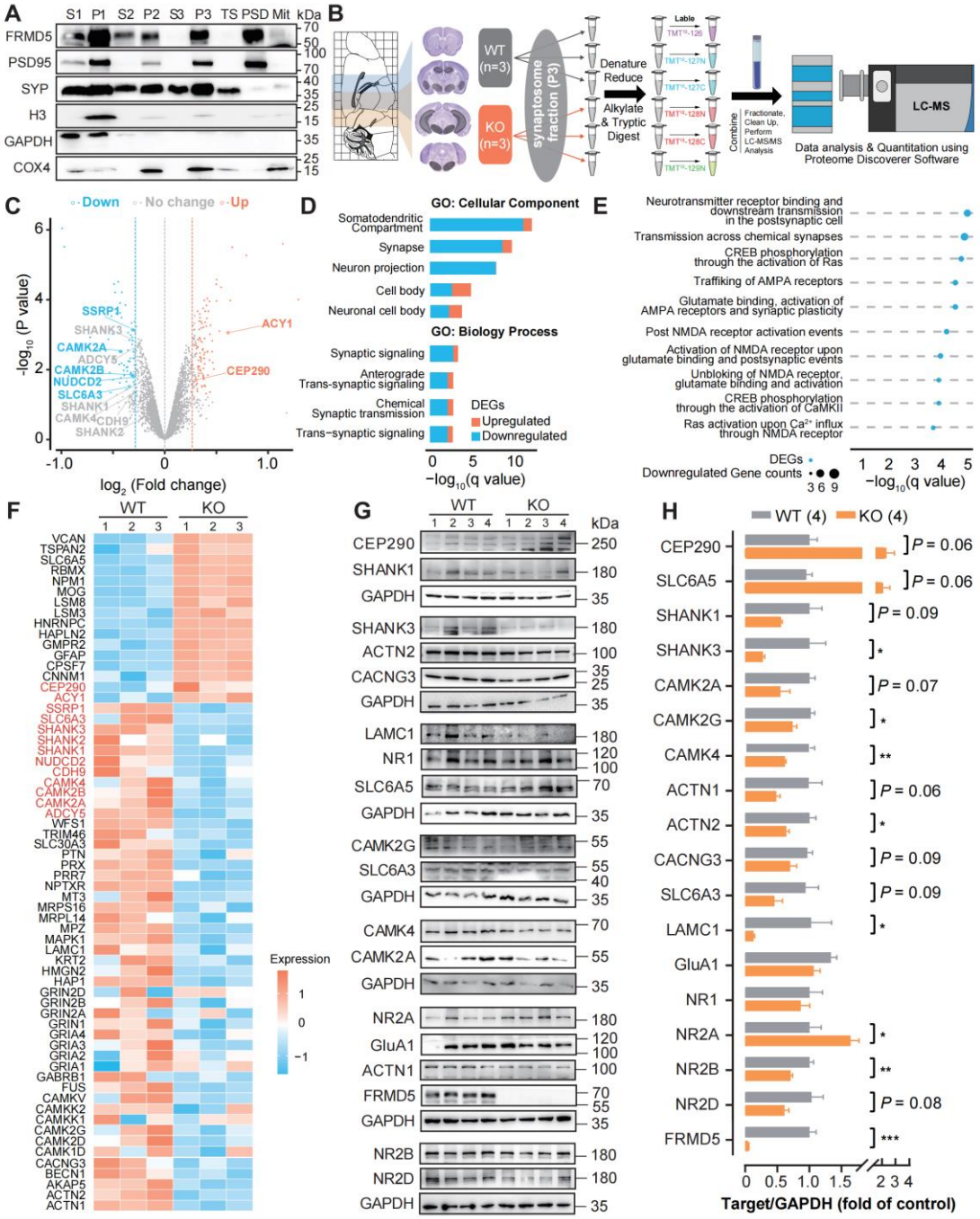
A
S1 P1 S2 P2 S3 P3 TS PSD Mit kDa
FRMD5
PSD95
SYP
H3
GAPDH
COX4
B
WT (n=3)
KO (n=3)
synaptosome fraction (P3)
Denature Reduce
Alkylate & Tryptic Digest
Label
Combine
Fractionate, Clean Up, Perform LC-MS/MS Analysis
LC-MS
Data analysis & Quantitation using Proteome Discoverer Software
C
Down
No change
Up
-log10 (P value)
log2 (Fold change)
SSRP1
SHANK3
CAMK2A
ADCY5
CAMK2B
NUDCD2
SLC6A3
SHANK1
CAMK4
CDH9
SHANK2
ACY1
CEP290
D
GO: Cellular Component
Somatodendritic Compartment
Synapse
Neuron projection
Cell body
Neuronal cell body
GO: Biology Process
Synaptic signaling
Anterograde Trans-synaptic signaling
Chemical Synaptic transmission
Trans-synaptic signaling
DEGs
Upregulated
Downregulated
−log10(q value)
E
Neurotransmitter receptor binding and downstream transmission in the postsynaptic cell
Transmission across chemical synapses
CREB phosphorylation through the activation of Ras
Traffiking of AMPA receptors
Glutamate binding, activation of AMPA receptors and synaptic plasticity
Post NMDA receptor activation events
Activation of NMDA receptor upon glutamate binding and postsynaptic events
Unbloking of NMDA receptor, glutamate binding and activation
CREB phosphorylation through the activation of CaMKII
Ras activation upon Ca2+ influx through NMDA receptor
DEGs
Downregulated Gene counts
−log10(q value)
F
WT
KO
VCAN
TSPAN2
SLC6A5
RBMX
NPM1
MOG
LSM8
LSM3
HNRNPC
HAPLN2
GMPR2
GFAP
CPSF7
CNNM1
CEP290
ACY1
SSRP1
SLC6A3
SHANK3
SHANK2
SHANK1
NUDCD2
CDH9
CAMK4
CAMK2B
CAMK2A
ADCY5
WFS1
TRIM46
SLC30A3
PTN
PRX
PRR7
NPTXR
MT3
MRPS16
MRPL14
MPZ
MAPK1
LAMC1
KRT2
HMGN2
HAP1
GRIN2D
GRIN2B
GRIN2A
GRIN1
GRIA4
GRIA3
GRIA2
GRIA1
GABRB1
FUS
CAMKV
CAMKK2
CAMKK1
CAMK2G
CAMK2D
CAMK1D
CACNG3
BECN1
AKAP5
ACTN2
ACTN1
Expression
G
WT
KO
kDa
CEP290
SHANK1
GAPDH
SHANK3
ACTN2
CACNG3
LAMC1
NR1
SLC6A5
CAMK2G
SLC6A3
CAMK4
CAMK2A
NR2A
GluA1
ACTN1
FRMD5
NR2B
NR2D
H
WT (4)
KO (4)
P = 0.06
P = 0.09
P = 0.07
P = 0.06
P = 0.09
P = 0.09
P = 0.08
Target/GAPDH (fold of control)

394

395

Figure 4. Molecular changes in the synaptosome of *Frmd5*$^{-/-}$ mice.

(**A**) Western blot results of cell components separated by gradient sucrose centrifugation. S1, cytoplasm and all membrane structure; P1, nucleus and nonlysis cells; S2, cytoplasm and light membrane structure; P2, crude synaptosomes; S3, synaptic vesicle component; P3, synaptosome and mitochondria; TS, presynaptic membrane component; PSD, postsynaptic density; Mit, mitochondria; PSD-95, postsynaptic membrane marker (postsynaptic density - 95); SYN, presynaptic membrane marker (synaptophysin); H3, nucleus marker (histone-3); COX4, mitochondrial marker (cytochrome c oxidase subunit 4). (**B**) Schematic diagram of tandem mass tag (TMT)-labeled quantitative proteomics. (**C**) Volcanic map of differentially expressed proteins identified by TMT proteomics. Labeled genes indicate the autism risk genes included in the SFARI database. (**D**) Top items in the GO enrichment analysis in cellular components and biological processes. (**E**) Top biological pathways enriched for differentially expressed proteins. (**F**) Heatmap of representative differentially expressed proteins in TMT proteomics. Red-labeled genes indicate the autism risk genes included in the SFARI database. (**G** and **H**) Western blot verification of differentially expressed proteins.

Data are represented as the means ± SEM. Unpaired t test in (H). *$P < 0.05$, **$P < 0.01$, ***$P < 0.001$.

Methods

Animals

C57BL/6J and ICR-strain mice. All mice were provided by the Animal Center of the Peking University Health Science Center. The mice were housed in 2-5 subjects per individually ventilated cage (IVC) with corn cob bedding. The mice were housed on a 12-hour light/dark cycle with food and water ad libitum. Both male and female C57BL/6J mice were used in the experiments. All animal studies were approved in accordance with the relevant guidelines of the Animal Center of the Peking University Health Science Center, including any relevant details.

Generation of *Frmd5* knockout mice. We used C57BL/6J transgenic mice to generate *Frmd5* knockouts with site-specific transcription activator-like effector nuclease (TALEN) technology. Several TALEN target sites were designed on exon 6 of the *Frmd5* gene, and the most effective binding site was as follows: *Frmd5*-T3-L, 5'-GAAGGCTACAGCTCCAA-3'; *Frmd5*-T3-R, 5'-CCAGTTTCTCTGAAT- GT-3'. Knockout of *Frmd5* was achieved by a frameshift mutation in *Frmd5* with a 1-bp (△1) or 2-bp (△2) deletion, which resulted in premature termination of the transcription translation process. The constructed TALEN plasmids were recovered by enzymatic digestion, followed by transcription *in vitro* to produce the target RNA. The RNA was injected into 0.5-day fertilized eggs by microinjection, which were transplanted into the ampulla of infusion tubes of pseudopregnant ICR mice for artificial implantation. Twenty-one days after the birth of the pups, tail tissue was collected for genomic DNA extraction and PCR amplification to perform sequencing analysis and genotyping. Because of the risk

of off-target effects with TALEN gene editing technology, off-target prediction was performed, and the results showed that no off-target effects were present (not shown). By analyzing the sequencing results, the protein after the frameshift mutation was truncated by only approximately 1/3 of the size of the original protein compared with the 570 amino acids of wild-type *Frmd5*. The resulting chimeric mice were bred with C57BL/6J mice to confirm germline transmission, and the genotypes were identified by PCR and capillary electrophoresis with three primers as follows: (1) Frmd5-STR-F, 5'-TGTAAAACGACGGCCAGTTACTTGT -GGCCTCCGAGAAC-3'; (2) Frmd5-STR-R, 5'-GGATCAC -CATTGCTGGGAGT-3'; and (3) M13F-FAM, 5'-TGTAAAACGACGGCCAGT-3', labeled with 6-FAM (6-carboxyfluorescein). The wild-type (WT) DNA resulted in a signal at 457 bp; the heterozygote (Het) DNA resulted in two signals at 457 bp with 456 bp (△1) or 455 bp (△2); and the knock-out (KO) DNA included three conditions: △1/△1, △1/△2, or △2/△2.

The resulting constitutive *Frmd5* deletion mice were bred as Het×Het or Het×KO for all experiments (since female parents were infertile, only male parents were used for breeding). The littermates derived from parental breeding and different litters but within 1 week of difference in date of birth were used as controls.

RNA isolation, reverse transcription, and quantitative real-time PCR

Different organ tissue samples from mice were collected in TRIzol reagent to protect RNA from degradation according to the manufacturer's protocol (Invitrogen). Then, total RNA was extracted with a standard phenol–chloroform protocol. Total RNA (2,000 ng) was reverse-transcribed into cDNA with a 5X All-In-One RT MasterMix Kit (Applied

Biological Materials Inc., Canada; G489). RT–qPCR was performed with a SYBR® Green Real-time PCR Master Mix Kit (TOYOBO, Japan; QPK-201) on an ABI 7500 Real-Time PCR system (Applied Biosystems, USA). The primers used in this study are listed as follows: (1) *Frmd5*-qPCR-F, 5'-GA -GTCCAGTGCCAAGATC-3'; (2) *Frmd5*-qPCR-R, 5'-GCCT TCCATGATAGAGATGT-3'; (3) *Gapdh*-qPCR-F, 5'-GGTGCTGAGTATGTCGTGGA -3'; and (4) *Gapdh*-qPCR-R, 5'- CCTTCCA -CAATGCCAAAGTT-3'. Gene expression levels of three technical replicates were normalized with the $2^{-\Delta\Delta CT}$ method, using *Gapdh* as the reference gene.

Western blot

Mice were deeply anesthetized by injection of 0.3~0.4 mL of 1% pentobarbital sodium, and the unresponsiveness of limbs in mice under a hemostatic clamp was considered the anesthesia eligibility criterion. The heart was exposed, and the right pericardium was clipped. Then, normal saline was rapidly bolus injected at the apical point of the left ventricle. The mice were systemically perfused to remove blood. Mice were immediately decapitated, and the brain tissues were rapidly isolated and stored at -80 ℃ after snap freezing in liquid nitrogen.

Frozen tissues were lysed in RIPA lysis buffer (Applygen Technologies, Beijing) and a protease inhibitor cocktail. The lysates were collected, and the supernatant was used to determine the protein concentration by BCA (Thermo Fisher Scientific, USA; 23225). Total protein was mixed with 5X SDS–PAGE Protein Sample Loading Buffer (Applygen Technologies, China; B1012-5) and heated at 95 °C for 5 min. Equal amounts of samples were separated by 10% SDS–PAGE and transferred to nitrocellulose membranes (Pall

Gelman Laboratory, USA), which were then blocked and incubated with primary antibodies overnight at 4 °C. After washing the membranes, they were incubated with horseradish peroxidase-conjugated secondary antibodies for 1 hour at room temperature, followed by additional washes. Bands were subsequently visualized on film using enhanced chemiluminescence reagents (Millipore, USA, WBKLS0500). Band intensities were quantified using ImageJ and statically analyzed by Prism. Detailed information on the primary and horseradish peroxidase (HRP)-labeled secondary antibodies is presented in Supplementary Table S5.

Behavioral experiments

The resulting constitutive *Frmd5* deletion mice were bred as Het×Het or Het×KO for all experiments (since female parents were infertile, only male parents were used for breeding). The littermates derived from parental breeding and different litters but within 1 week of difference in date of birth were used as controls.

Open Field Test

The apparatus was a white plastic open field with a square floor (50 cm × 50 cm) and surrounding walls (50 cm high). Each mouse was gently placed in the center of the open field and videotaped for 30 min. The total distance mice traveled was measured using SMART software (version 3.0, PanLab, Barcelona, Spain).

Elevated O-maze test

The elevated O-maze is a circular platform 60 cm above the ground with a ring width of 6 cm. It consists of two relatively closed quadrants and two open quadrants. Mice were placed facing the open quadrants, and their behavior was monitored for 5 min with SMART

3.0 software and assessed based on the distance, the times of entering the open quadrants and time spent in the open quadrants of the maze.

Rotarod Test

In the training session, mice were placed on a rotarod moving at 4 rpm and trained to stay on the rotarod for at least 3 min. On the second day, mice ran their full rotarod test. The rotarod began at 4 rpm and accelerated to 40 rpm over 5 min. The latency to fall off was recorded. The examination was repeated four times with at least a 30 min interval.

Three-chamber social test

The apparatus consisted of a rectangular box with three separate chambers (20 × 45 × 20 cm each). One side of each chamber contained a circular metal wire cage (stimulus animal cage, 10 cm high and 8 cm in diameter). One day before the test, all subjects were habituated to the arena for 5 min and recorded to determine their preferences on both sides of the box. Age- and sex-matched unfamiliar stimulus voles were also habituated to the wire cages for 5 min. On the testing day, the test mice were first placed in the middle chamber and allowed to explore the entire test chamber for 5 minutes. Immediately after the 5 min period, the test mice were placed in a clean holding cage, and a male mouse (stranger 1) with no prior contact with the test mice was enclosed in one of the wire cages. Next, the test mice were returned to the middle chamber and allowed to explore for 5 minutes. After the test session, the test mice were again placed in the holding cage, and a second unfamiliar mouse (stranger 2) was enclosed in the wire cage on the opposite side. The test mice were placed in the middle chamber and had a choice between the first, already investigated unfamiliar mouse and the novel unfamiliar mouse for 5 minutes. The

time spent in each chamber, the time spent around each cage and the total distances of movement were automatically measured from images using Smart 3.0 software.

Olfactory habituation/discrimination

The experiment was carried out in a standard mouse cage (30 cm × 20 cm × 13 cm). Purified water, bitter almond flavor and banana flavor were prepared as three kinds of nonsocial taste stimulation. Two pads containing feces of mice from different cages were prepared and soaked in water to produce extracts for social olfactory stimulation. The mice were placed in the cage for free exploration for 5 min. Cotton swabs dipped in an odorous liquid were fixed on a clean cage lid. The test mice were allowed to move freely in the cage for 2 min each time. Each olfactory stimulus was repeated 3 consecutive times, and another olfactory stimulus was replaced at an interval of 1 min. From the side, the camera recorded how long the mice spent sniffing and nibbling at each scent.

Self-grooming test

The standard mouse cage (30 cm × 20 cm × 13 cm) was added to an approximately 1 cm thick wood chip cushion. During the experiment, the mice were placed into the cage and moved freely. A 15 min video was recorded by Smart software. The first 5 min was the adaptation stage, and the times and duration of self-grooming in the last 10 min were analyzed and counted manually.

Spontaneous motor stereotypies

The tested mice were placed into the open field to move freely, and the behaviors of the tested mice were recorded for 30 minutes with the camera directly above the open field. The times of looking-out (standing up in place), climbing the wall (standing with lower

limbs and upper limbs resting on the sidewall) and jumping were manually counted.

Pup mouse ultrasonic vocalization test

A clean, lidless feeding cage was placed in the soundproof test box. A capacitive microphone (CM16/CMPA, Avisoft Bioacoustics) was suspended 25 cm above and connected to an AUSG-116H amplifier (Avisoft Bioacoustics). The sampling frequency was set at 250,000 Hz. A 7-day-old baby mouse was gently removed from the original feeding cage and placed in a clean cage without a lid. After 1 min of adaptation, the sounds produced within 5 min were recorded and analyzed by SASLab Pro software (Avisoft Bioacoustics). The frequency of vocalization, the average duration of each vocalization, the latency of the first vocalization and the peak frequency of each vocalization were recorded. After the 5 min recording, the pup mice were numbered and genotyped to distinguish individual mice.

Novel object and place/position recognition test

The new object recognition experiment was carried out in an open field test chamber (50 cm × 50 cm × 50 cm). During the object recognition test, the tested mice first adapted to the open field environment for 10 minutes, and then two familiar objects were placed in opposite corners of the open field. The tested mice were allowed to explore freely for 10 minutes, and one object was changed into a new object after an interval of 60 minutes. The tested mice were allowed to explore freely for 10 minutes. During the place/position recognition test, the tested mice first adapted to the open field environment for 10 minutes, and then two identical objects, mineral water bottles filled with bromophenol blue, were placed in the corners of the open field's sides. The tested mice were allowed to explore

freely for 10 minutes, and one object was moved to the opposite corner of the other objects after an interval of 60 minutes. The tested mice were allowed to explore freely for 10 minutes. The camera connected to the behavioral analysis software Smart 3.0 recorded and automatically analyzed the time the tested mice spent exploring around the two objects. The new/old object was a mineral water bottle filled with bromophenol blue or a round metal that could be filled with liquid.

Y-maze test

The Y-maze test apparatus is composed of three closed arms with the same angle of 120°. Each arm is 50 cm × 8 cm × 15 cm (length × width × height) and has a movable partition in the center. In the experimental paradigm of the working memory test, each mouse was randomly placed into any arm of maze Y to explore freely for 8 minutes, the activity of the mouse in the Y-maze was recorded by the camera directly above, and the spontaneous alternating behavior of the mouse was analyzed. In the spatial memory test paradigm, one of the arms of the Y-maze was randomly closed (novel arm); each tested mouse was allowed to explore the other two arms for 10 min, and the baffle was removed after 60 min. Once again, the tested mice were allowed to explore the three arms freely for 10 minutes to test their spatial memory. The video camera above recorded the activity of the mice in the Y maze. The behavioral analysis software Smart 3.0 was used to analyze the time and number of mice entering the new arm.

Morris water maze test

The water maze is a circular tank with a diameter of 120 cm and a depth of 60 cm. Different visual clues were pasted around the tank, which served as spatial landmarks for the mouse.

The water maze was divided into four quadrants, the target quadrant, and three nontarget quadrants. On Day 0, mice were trained to find the platform with a visible flag. On Days 1–6, the platform was submerged 1–2 cm below the water surface. Mice were placed into the maze in one of four quadrants, facing the wall of the tank, and allowed to search for the platform for 60 s. Four trials a day were conducted with a 45-min interval between trials, and escape latency was recorded. A spatial memory test was performed on day 7 with the platform removed, occupancy time (%) in the target quadrant was compared with all other quadrants, and the platform crossings in the target quadrant were compared with a similar area in all other quadrants. The moving distance, speed, latency to reach the platform and duration of stay at each quadrant were analyzed by Supermaze software.

Hot plate test

Mice were placed on a hot plate (IITC Life Science) set at 55 ± 1 ℃, and the latency to hind paw licking was recorded.

Von Frey test

Mice were placed in a plastic cage with a metal mesh floor, and the plantar surface of the hind paw was stroked using von Frey filaments (IITC Life Science) for 3 s twice. The mechanical threshold was determined by Dixon's up-and-down method.

Golgi-Cox staining

Golgi-Cox staining was carried out using the Hito Golgi-Cox OptimStain^{TM} Kit (HITO, cat: HTKNS1125) according to the manufacturer’s instructions. The brains were harvested and maintained in the fixed working solution (Solution-1: Solution-2=1:1) in the dark for two weeks at room temperature and carefully transferred and maintained in 5 ml Solution-

3 for 48 hours at 4℃. After freezing at -20 °C, the sample was cut into slices and immediately stained. For dehydration, the sections were treated with gradient ethanol and xylene and then sealed with neutral balsam. Images were captured under a confocal fluorescence microscope (TCS SP8, Leica, Germany) at 2-μm intervals. The semiautomatic mode of Imaris 9.0 software was used to conduct 3D tracking and reconstruction of the neurons photographed under a confocal microscope. The Sholl analysis function of the software was used to analyze the complexity of neuronal dendrites with the Sholl radius defined as 1 μm.

Sparse labeling and dendritic spine density analysis

The mice were anesthetized by i.p. injection of pentobarbital sodium. The adeno-associated viruses (AAVs) were injected into the hippocampal dentate gyrus (DG) (Bregma AP: −1.94 mm, ML: ±1.25 mm, DV: −1.75 mm), with a volume of 0.1 μ L containing pAAV-CAMKIIα-CRE (1×10^7, BrainVTA, Wuhan) and pAAV-hsyn-dio-EGFP (1×10^7, BrainVTA, Wuhan). After 3 weeks, the brains were extracted, fixed in 4% PFA overnight at 4 °C, and dehydrated in 20% and 30% sucrose in PBS buffer. Consecutive 300 μm brain slices were washed with PBS 3 times. Dendritic spines in the hippocampal DG region were visualized by a confocal microscope (TCS SP8, Leica, Germany).

For dendritic branch complexity analysis, Z-stacks consisted of scans at 2-μm intervals to image granulosa cells in the DG region. The semiautomatic mode of Imaris 9.0 software was used to conduct 3D tracking and reconstruction of the neurons photographed under a confocal microscope. The Sholl analysis function of the software was used to analyze the complexity of neuronal dendrites with the Sholl radius defined as 1 μm.

For dendritic spine morphological analysis, Z-stacks consisted of scans at 0.1-μm intervals to image granulosa cells in the DG region. The width of the spine head and spine neck of each dendrite were measured using a semiautomatic program of ImageJ and classified as branched (manually classified), filopodia/dendrite (length > 2 && length ≤ 5), mushroom (head ≥ 1.5*neck), long thin (head <1.5*neck && length >2*head) or stubby (head <1.5*neck && length ≤ 2*head).

In utero electroporation

Embryonic day (E) 14.5 embryos from wild-type ICR mice provided by the Department of Laboratory Animal Science, Peking University Health Science Center, were used for the experiment. EYFP plasmid (1 μg/μL) was injected into the lateral ventricles. The brains of electroporated embryos were harvested 2, 3 or 4 days postinjection and then sliced and scanned using the virtual slide system VS120 (OLYMPUS, Japan).

Cell culture and transfection

Hippocampal neurons were obtained from embryonic Day 16.5 mouse embryos and plated onto 35-mm dishes coated with poly-D-lysine (Sigma Aldrich) at an appropriate density. After 4 h in plating media (10% fetal bovine serum in DMEM), the cultures were transferred to neurobasal medium supplemented with 2% B27 and 0.5 mM GlutaMAX-I (Gibco Invitrogen). Half of the medium was replaced with fresh medium every 3 days. At day *in vitro* (DIV) 3, cytosine arabinoside (Sigma Aldrich) was added to the maintenance medium at a final concentration of 10 μM to inhibit glial proliferation.

For morphological experiments, hippocampal neurons were transfected with the indicated plasmids (p-EGFP-N1, p3xFLAG-CMV-10-vector, p3xFLAG-human-FRMD5-CMV-10

and pEGFP-C3-human-FRMD5) using Lipofectamine™ 2000 Transfection Reagent (Invitrogen™) following the manufacturer's guidelines and harvested for morphological analyses after 2-3 days.

Immunofluorescence staining

Cells were fixed with 4% paraformaldehyde after being washed twice with 1x PBS and maintained in 0.3% Triton X-100/1x PBS for 20 min at room temperature. After another 3 washes with 1x PBS, the cells were blocked with 5% bovine serum albumin (BSA) and 0.3% Triton X-100 in 1x PBS before incubation with a primary antibody overnight at 4 °C. Cells were washed in 1x PBS before incubation with secondary fluorescent antibody. Coverslips were mounted onto slides in antifade (Solarbio, C0031) containing Hoechst 33342.

Whole-cell patch clamp recordings

Current-clamp recording was performed to record APs at least 1 hour after neuron plating. The intracellular solution contained (mM) 130 K-gluconate, 5 NaCl, 10 Na-phosphocreatine, 0.02 EGTA, 1 $MgCl_2$, 10 HEPES, 2 Mg-ATP, 0.2 Na_2-ATP and 0.10% Biocytin (pH 7.3, 290-320 mOsm/L). Whole-cell currents were recorded using an EPC-10 amplifier (HEKA, Germany) at a 5-10 kHz sample rate and were low-pass filtered at 2-5 kHz. The series resistance was 10-20 MΩ and was compensated 80-90%. The data were acquired by the PatchMaster program (HEKA, Germany). The sEPSC frequency and amplitude were detected and analyzed using Mini Analysis, and the differences between the groups were detected by unpaired t test. The nonparametric Kolmogorov–Smirnov test was used for the distribution probability curves of the peak-to-peak interval and amplitude.

Synaptic fractionation

Brain tissues were homogenized in 0.32 M sucrose in 4 mM HEPES (pH 7.4) for 2 min using a tissue homogenizer. The supernatant (S1) was collected after low-speed centrifugation at 900 × g for 10 min at 4 °C and resuspended in 500 μl 0.32 mol/L sucrose HEPES solution to obtain the nuclear components (P1). Then, S1 was centrifuged at 10,000 × g for 15 min to yield the crude synaptosome fraction (P2) and cytosol/light membranes in the supernatant (S2). The P2 pellet was lysed in ddH2O by hypo-osmotic shock and centrifuged at 25,000 × g for 20 min to obtain pelleted synaptosomes (P3) and vesicular fraction (S3). The supernatant (S3) was collected and stored at -80 °C, and pelleted synaptosomes were resuspended in 0.32 mol/L sucrose HEPES solution. The discontinuous sucrose gradient consisted of 3.5 ml 1.2 mol/L sucrose HEPES solution, 3.0 ml 1.0 mol/L sucrose HEPES solution and 3.0 ml 0.8 mol/L sucrose HEPES solution. Synaptosomes (P3) were layered on top of the discontinuous sucrose gradient. The SPM fraction was collected by an 18 G needle and 1 ml syringe at 1.0 M/1.2 M sucrose HEPES solution interface, and the mitochondrial fraction (Mit) was collected by an 18 G needle and 1 ml syringe at 0.8 M sucrose HEPES solution interface after ultracentrifugation of the gradient at 150,000 × g for 2 hours. SPM was collected and pelleted by ultracentrifugation at 200,000 × g for 30 min. To prepare the PSD fraction, SPM was incubated in 0.54% Triton X-100 for 15 min followed by centrifugation at 32,000 × g for 20 min.

Tandem mass tag (TMT) quantitative proteomic analysis

An equal amount of protein (50 μg) was extracted from each sample, reduced with 1 mM DTT for 1 h, and then alkylated with 5.5 mmol/L TCEP for 40 min in the dark. The protein

was then digested overnight at 37 °C with sequence-grade modified trypsin. After desalination with a C18 Sep-Pak filter, the peptides were labeled and combined with TMT hexadecimal labeling reagent. The TMT-labeled peptide complexes were then separated by HPLC and collected for LC–MS/MS analysis.

In the operation of the LC–MS/MS analyzed Thermo Scientific QE-HFX mass spectrometer, the peptides were separated by gradient elution using the Thermo Scientific Dionex Ultimate 3000 HPLC system at a flow rate of 0.30 μl/min for a total of 2 hours before use in the Thermo Scientific QE-HFX mass spectrometer. The mass spectrometer analytical column is a homemade fused quartz capillary column filled with C-18 resin. The mobile phase consisted of 0.1% formic acid, and mobile phase B consisted of 80% acetonitrile and 0.1% formic acid. The QE-HFX mass spectrometer uses Xcalibur software to operate in data-dependent acquisition mode and has a full-scan mass spectrometer in orbit. Then, 20 data-dependent MS/MS were scanned with a normalized collision energy of 32%. The MS/MS protein map for each LC–MS/MS run was searched from mouse.fasta (UniProt) using the internal proteome discovery program (Version PD2.2, Thermo-Fisher Scientific, USA).

Bioinformatics analysis of differential proteins

The abundance values output by proteomics were normalized by the variance stable normalization (VSN) method to identify differential proteins. To adjust the samples to the same scale with a set of parameter transformations and maximum likelihood estimates, the abundance matrix with all samples was fed from the R-packet VSN to the justvsn function. The $\log_2$ transformation matrix from VSN was fitted to multiple linear models for

differential protein analyses by the weighted least square method (lmFit function from limma software package). Proteins with a P value less than 0.05 and an absolute log2 (fold change) greater than 0.3 were selected as differential proteins. Downregulated and upregulated proteins were used for pathway and GO analysis in the ToppGene network tool, respectively.

Statistical analyses

All data are presented as the means ± SEM. Statistical analyses were performed using Prism 8.0 software (GraphPad Software, La Jolla, CA, USA). Biochemical experiments were measured by optical density using ImageJ, and the bar chart represents the average data of at least three independent experiments. The normal distribution test (D 'Agostino-Pearson omnibus normality test) and the homogeneous variance test (F test) were conducted to ensure that the subsequent tests could be completed using the parameter test method. According to the number of factors and whether the pairing was reasonable, the t test or analysis of variance (ANOVA) method was selected for statistical analysis. Tukey's or Bonferroni's method was used for the posttest. Statistical significance was set at $P < 0.05$.

Behavioral experiments obtained target behavioral parameters through SMART 3.0 software and a built-in threshold calculation formula. All experiments were repeated at least three times. Some elements of the behavior pattern diagram are referred to Smart Servier Medical Art (smart.servier.com). The site's materials follow the Creative Commons Attribution 3.0 Unported License.

Acknowledgments

This work was supported by grants from the National Natural Science Foundation of China (31720103908, 82230094, 81621063) and by grants from the Ministry of Science and Technology of China (2022YFA1104003, 2021ZD0203204, 2021YFC2501003, and 2017YFA0701302).

Author contributions

H.Q. Z., Y. W. conceived and supervised the project. T.J. L., J. M., C. L., J.D., D.C. W., X.Y. Z. performed the behavioral, molecular and biochemical experiments, and G.G. X., C. C., N.Y. L. performed electrophysiology, morphology, and proteomics experiments; X.Y. Z., Y.N. X., T.J. L, J.M. wrote the manuscript. All authors have read and accepted the manuscript.

Competing interest declaration

The authors have declared that no conflicts of interest exist.

Additional information

Study approval

All animal procedures performed in this study were approved by the Ethics Committee of Peking University Health Science Center (Beijing, China).

For the data from the Decipher project, those who carried out the original analysis and collection of the data bear no responsibility for the further analysis or interpretation of the data.

Extended data figure/table legends

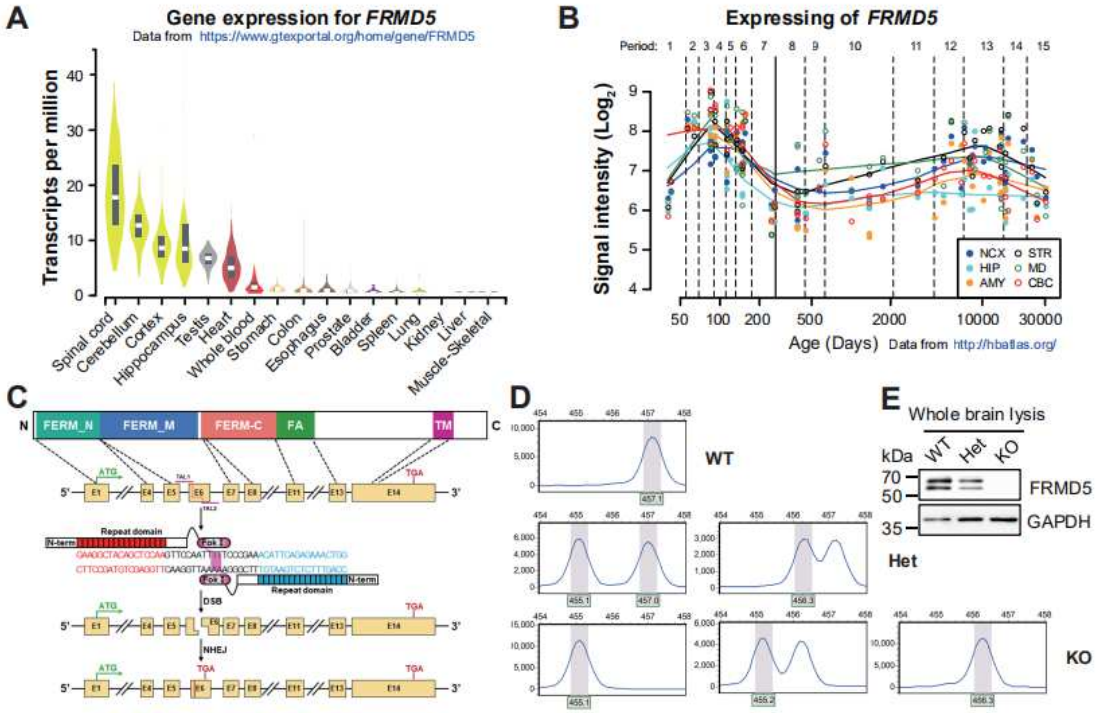

Figure S1. Expression of *FRMD5* in humans and the *Frmd5*$^{-/-}$ mouse line.

(**A**) Gene expression of *FRMD5* in humans. (**B**) Expression of *FRMD5* during the life span of humans. (**C**) Schematic diagram of building the *Frmd5*$^{-/-}$ mouse line. (**D**) Genotype identification by PCR capillary electrophoresis. (**E**) Western blot for WT, *Frmd5*$^{+/-}$ and *Frmd5*$^{-/-}$ mice.

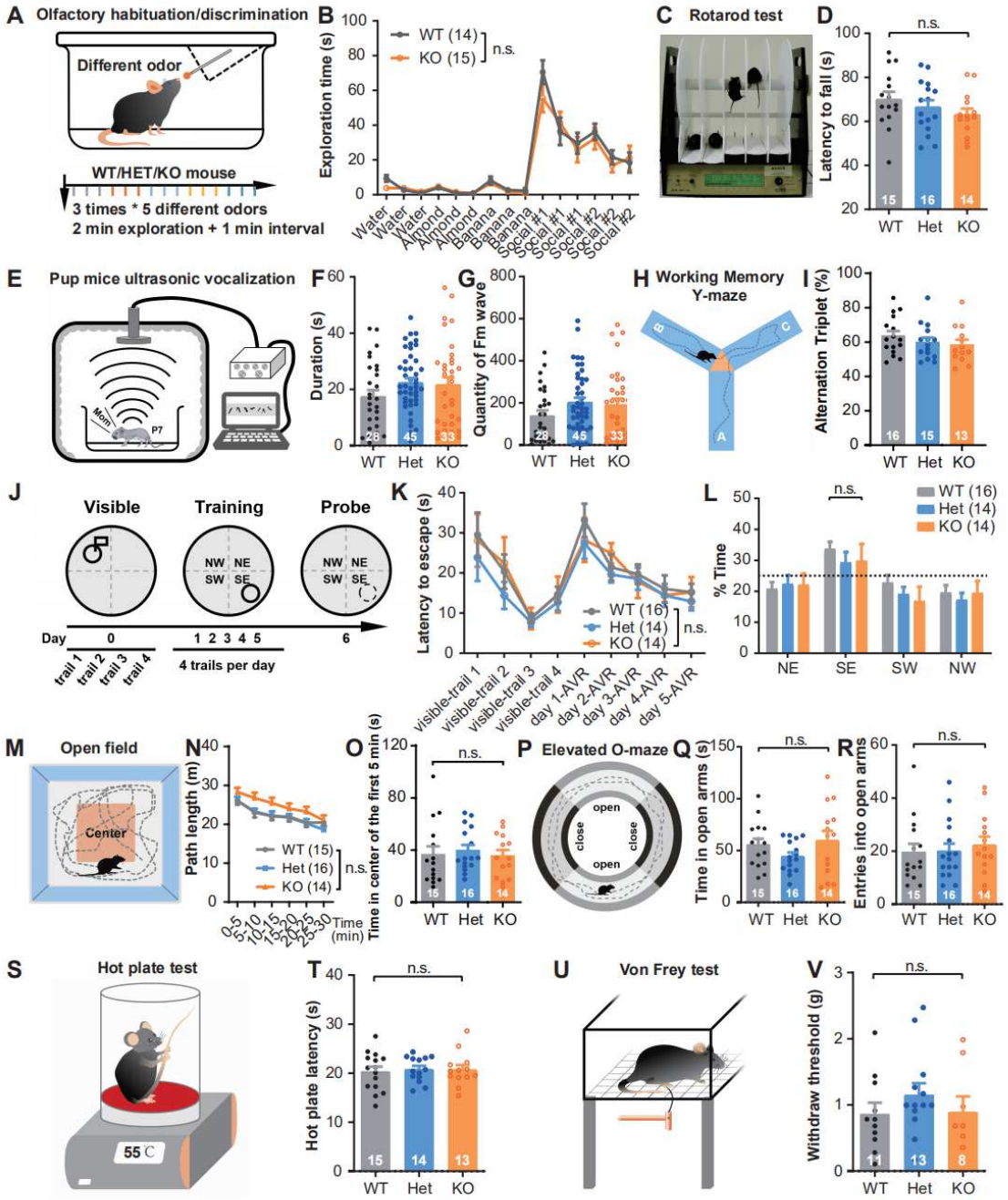
A Olfactory habituation/discrimination
Different odor
WT/HET/KO mouse
3 times * 5 different odors
2 min exploration + 1 min interval
B
Exploration time (s)
WT (14)
KO (15)
n.s.
Water
Almond
Banana
Social #1
Social #2
C Rotarod test
D
Latency to fall (s)
n.s.
WT Het KO
E Pup mice ultrasonic vocalization
Mom
P7
F
Duration (s)
G
Quantity of Fm wave
H Working Memory
Y-maze
I
Alternation Triplet (%)
J
Visible
Training
Probe
NW NE
SW SE
Day
trail 1
trail 2
trail 3
trail 4
4 trails per day
K
Latency to escape (s)
visible-trail 1
visible-trail 2
visible-trail 3
visible-trail 4
day 1-AVR
day 2-AVR
day 3-AVR
day 4-AVR
day 5-AVR
L
% Time
WT (16)
Het (14)
KO (14)
NE SE SW NW
M Open field
Center
N
Path length (m)
WT (15)
Het (16)
KO (14)
Time (min)
O
Time in center of the first 5 min (s)
P Elevated O-maze
open
close
Q
Time in open arms (s)
R
Entries into open arms
S Hot plate test
55 C
T
Hot plate latency (s)
U Von Frey test
V
Withdraw threshold (g)

775

776

Figure. S2. Knockout of Frmd5 does not affect olfactory sensation, motor function, language function, working memory, anxiety or nociception.

(**A**) Schematic diagram of olfactory adaptation and discrimination experiment. (**B**) Exploration time of olfactory stimulus. (**C**) Schematic diagram of the rotarod test. (**D**) Latency to fall in the rotarod test. (**E**) Schematic diagram of pup mouse ultrasonic vocalization. (**F** and **G**) Duration and quantity of Fm waves of pup mouse ultrasonic vocalization. (**H**) Schematic diagram of working memory in the Y-maze test. (**I**) Alternation triplet of working memory in the Y-maze test. (**J**) Schematic diagram of the Morris water maze. (**K** and **L**) Latency to escape and time spent in each zone of the water maze. (**M**) Schematic diagram of the open field test. (**N** and **O**) Path length and time in the center of the first 5 minutes of the open field test. (**P**) Schematic diagram of the elevated O-maze. (**Q** and **R**) Time spent in the open arms and entries into open arms of the elevated O-maze. (**S**) Schematic diagram of the hot plate test. (**T**) Hot plate latency in the hot plate test. (**U**) Schematic diagram of the von Frey test. (**V**) Withdrawal threshold of the von Frey test.

Data are represented as the means ± SEM. One-way ANOVA with Tukey's multiple comparisons test in (D), (F), (G), (I), (L), (O), (Q), (R), (T), and (V). Two-way ANOVA with Tukey's multiple comparisons test in (B), (K), and (N). n.s., no significant difference.

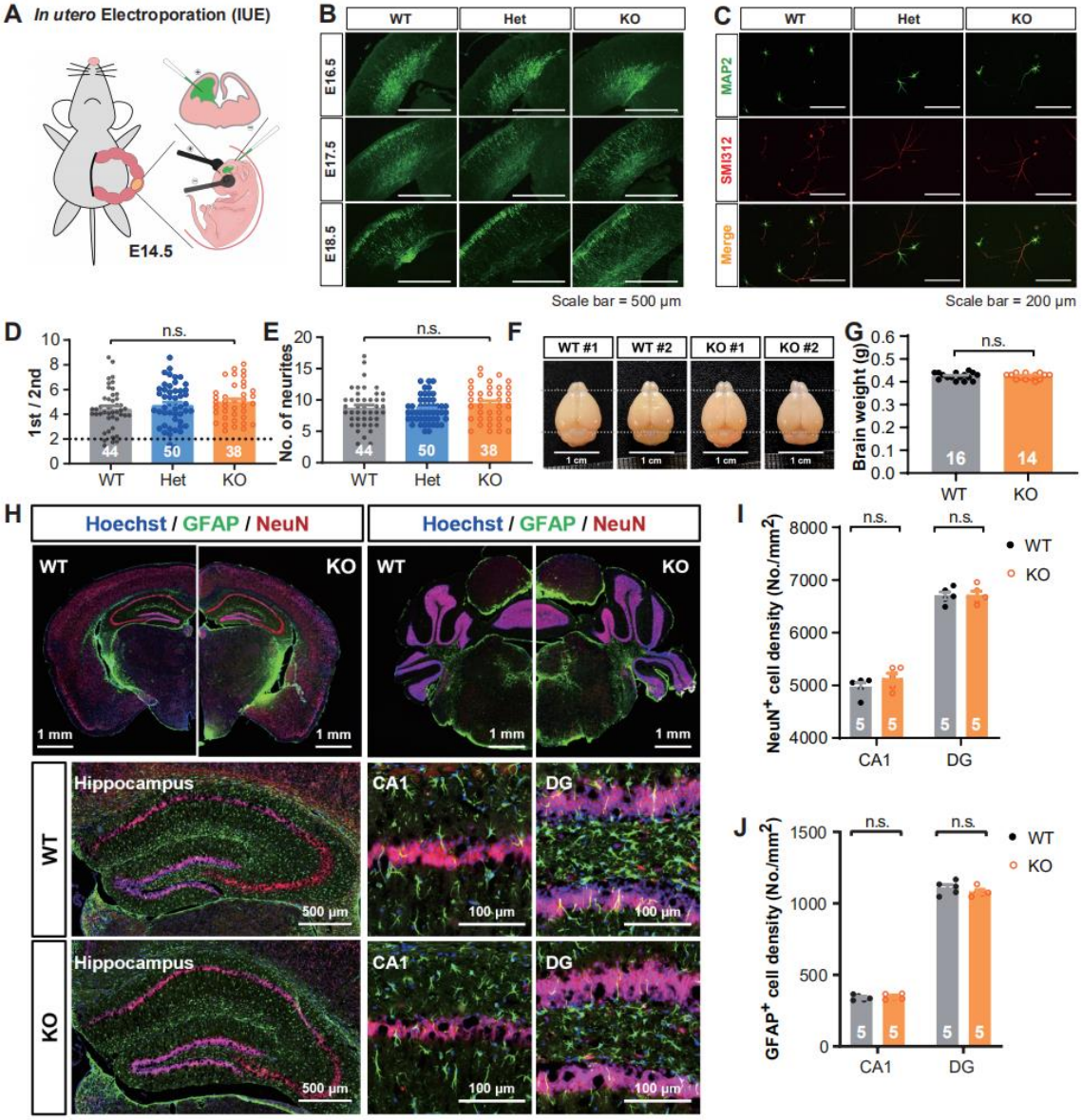
A In utero Electroporation (IUE)
E14.5
B
WT
Het
KO
E16.5
E17.5
E18.5
Scale bar = 500 μm
C
MAP2
SMI312
Merge
Scale bar = 200 μm
D
1st / 2nd
n.s.
44
50
38
E
No. of neurites
F
WT #1
WT #2
KO #1
KO #2
1 cm
G
Brain weight (g)
16
14
H
Hoechst / GFAP / NeuN
1 mm
Hippocampus
CA1
DG
500 μm
100 μm
I
NeuN+ cell density (No./mm2)
CA1
DG
J
GFAP+ cell density (No./mm2)

796

797

Figure. S3. Knockout of *Frmd5* does not affect cortical development or the percentage of neurons and astrocytes in the hippocampus.

(**A**) Expression of FRMD5 in the central nervous system and specific regions of the hippocampus. FRMD5 is highly expressed in the hippocampus, especially in the CA1 and DG. (**B**) Schematic diagram of *in utero* electroporation (IUE) in E14.5 mice. (**C**) Diagram of GFP-labeled cortical neuronal migration. Scale bar = 500 μm. (**D**) Diagram of staining of primary cultured DIV3 neurons. Scale bar = 200 μm. (**E**) The ratio of the longest axon marker SMI312 to the second longest dendrite marker MAP2. (**F**) Comparison of the number of neurites around the cell body. (**G**) Diagram of brain morphology of mice. Scale bar = 1 cm. (**H**) Brain weights of WT, Het and KO mice. (**I**) Diagram of staining for neuron markers (NeuN) and astrocyte markers (GFAP) in the CA1 and DG of the hippocampus. (**J** and **K**) Cell density of $NeuN^+$ and $GFAP^+$ neurons.

Data are represented as the means ± SEM. Unpaired t test in (H), (J) and (K); one-way ANOVA with Tukey's multiple comparisons test in (E) and (F). n.s., no significant difference.

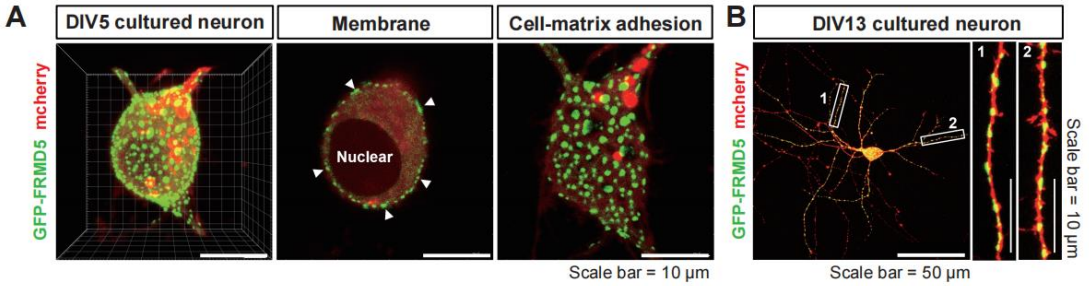

Figure. S4. FRMD5 is located on the cell membrane, cell-matrix adhesion, neuronal dendritic shaft, dendrite branch point, and the basilar part of the dendritic spine.

(**A**) Diagram of live cell imaging of primary cultured DIV5 hippocampal neurons. Scale bar = 10 μm. (**B**) Diagram of live cell imaging of primary cultured DIV13 hippocampal neurons. Scale bar = 50 μm & 10 μm.

822 **Figure. S5 Graphical abstract**

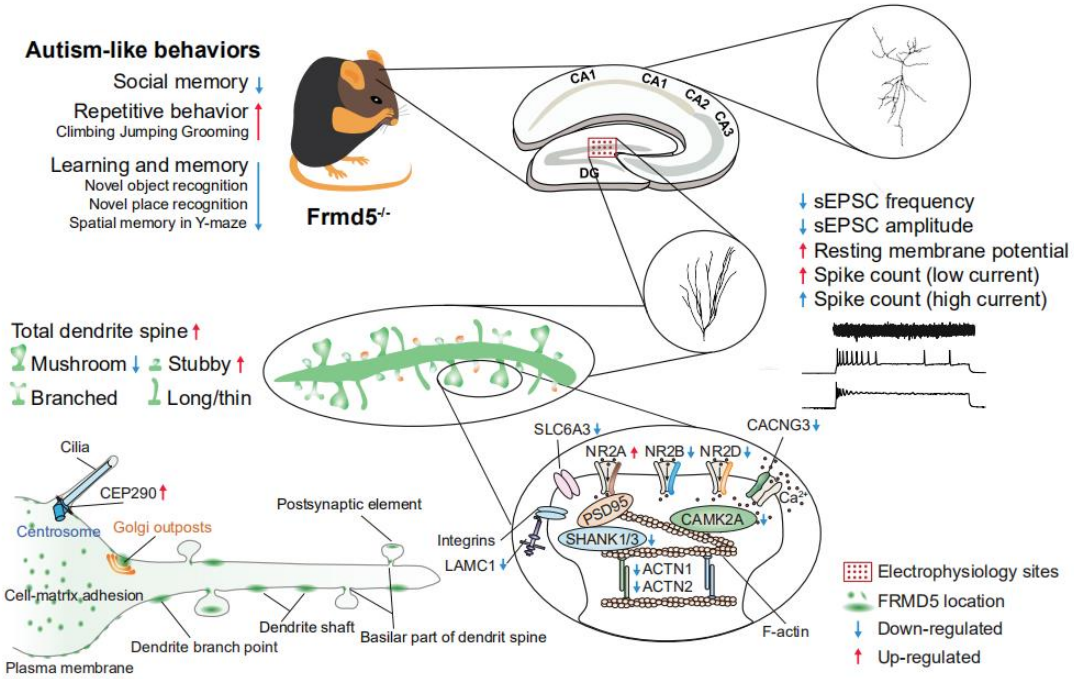

823

824

Table S1 FRMD5 deletion/mutation probands display a spectrum of neurodevelopmental phenotypes

ID	ClinVar -SCV002587810.1*	ClinVar -SCV002564148.1	ClinVar -SCV002564147.1	ClinVar -SCV000298972.1	Decipher -351796	Decipher -413294	Decipher -400953	Decipher -1392	GeneMatcher-1	GeneMatcher-2
Age (last assessment)	15.5 years	10 years	10 years	Unknown	6 years	10 years	5 years	19 years	1 year	Unknown
Sex	46XY	46XY	46XY	46XX	46XY	46XY	46XX	46XX	Unknown	Unknown
Allele	Heterozygous /SNP (missense)	Heterozygous /SNP (missense)	Heterozygous /SNP (missense)	Heterozygous /deletion	Heterozygous /deletion	Heterozygous /deletion	Heterozygous /deletion	Heterozygous /deletion	Heterozygous /SNP (missense)	Heterozygous /SNP (missense)
Variant/deletion	Chr15(GRCh38): g.43873961A>G, p.Tyr546Cys	Chr15(GRCh38): g.43873961A>G, p.Tyr546Cys	Chr15(GRCh38): g.43883793A>C, p.Ser349Arg	Chr15(GRCh37): 44484701 -47475522	Chr15(GRCh38): 43756117 -47706812	Chr15(GRCh38): 41529554 -48250359	Chr15(GRCh38): 43423101 -44571031	Chr15(GRCh38): 40993156 -45534313	Chr15(GRCh38): g.43874114T>C, p.(Asn495Ser)	Chr15(GRCh38): g.43883793A>C, p.Ser349Arg
Variant size	1 bp	1 bp	1 bp	2.99 Mb	3.95 Mb	6.72 Mb	1.15 Mb	4.54 Mb	1 bp	1 bp
Variant detection	WES	Unknown	Unknown	Unknown	Unknown	Unknown	Unknown	Unknown	Unknown	Unknown
Inheritance	Unknown	Unknown	Unknown	Unknown	De novo	Unknown	De novo	De novo	Unknown	De novo
Ethnicity	Unknown	Unknown	Unknown	Unknown	Unknown	Unknown	Unknow	Unknow	Unknown	Unknow
Pathogenicity /Contribution	Pathogenic Full	Uncertain significance	Uncertain significance	Uncertain significance	Likely pathogenic Full	Pathogenic Full	Likely pathogenic	Unknow	Unknown	Likely pathogenic Full
Craniofacial dysmorphism	Yes	No	Yes	No	No	No	Yes	No	Unknown	Yes
Head circumference	Unknown	Unknown	Unknown	Unknown	Unknown	Unknown	Unknown	Unknow	Unknown	Yes
Intellectual disability	Yes	No	Yes (mild)	No	No	Yes (mild)	Unknown	Yes	Yes	Yes
Developmental delay	Yes	Yes	Yes	No	No	No	No	No	Yes	Yes
ASD	**Yes**	**Yes**	**No**	**Yes**	**Yes**	**No**	**No**	**No**	**Unknown**	**No**
ADHD	No	No	No	Yes	No	Yes	No	No	Unknown	No
Other psychiatric	No	Unknow	Aggressive behavior	Oppositional defiant disorder Anxiety	No	No	No	No	Unknown	Unknown
Speech delay	No	Yes	No	No	Yes	No	Yes	Yes	Unknown	Yes
Speech apraxia	No	No	No	No	No	No	No	Yes	Unknown	No
Motor delay	Yes	Yes	Yes	No	No	No	Yes	No	Unknown	Yes
Motor dyspraxia	Yes	Yes	Yes	No	No	Yes	Yes	Unknown	Unknown	Yes
Other neurologic	Delayed myelination Nystagmus Seizures (EEG anomalies)	Delayed myelination EEG with focal spikes	Cerebellar ataxia Nystagmus and Opsoclonus Atypical absence seizure Headache	Unknown	Polyphagia	Unknown	Unknown	Unknown	Complete corpus Callosumagenesis	Cerebral atrophy Abnormality of eye movement
Other phenotype	Hypotonia Spasticity Renal anomalies	Spasticity Bruxism Failure to thrive Renal anomalies Short stature	Tics Gait ataxia	Unknown	Brachydactyly	Unknown	Hypertelorism, Recurrent infections, 2-3 toe syndactyly Polyhydramnios	Feeding difficulties in infancy Truncal obesity Hypotonia	Cryptorchidism Hypertonia	Muscular hypotonia Microcephaly
Contact information	hbellen@bcm.edu*	mokry@bcm.edu	mokry@bcm.edu	jhoffman@genedx.com	Decipher	Decipher	Decipher	Decipher	boriskerenyuen @gmail.com	Sonja.Neuser @medizin.uni-leipzig.de

Patients were collected from the ClinVar project (www.ncbi.nlm.nih.gov/clinvar), the DECIPHER project (www.deciphergenomics.org), and the GeneMatcher online resource (genematcher.org).

ASD, autism spectrum disorder; ADHD, attention deficit hyperactivity disorder; WES, whole-exome sequencing; SNP, single nucleotide polymorphism

* This patient has been reported previously. (Lu S, et al. Am J Hum Genet. 2022 Oct 6;109(10):1932-1943. doi: 10.1016/j.ajhg.2022.09.005.)

Table S2 Summary of ASD-like behavior tests

Phenotype	Assay	WT	Het	KO
Social behavior	home cage social interaction	−	−	−
	three chamber test			
	social preference	−	−	−
	social memory	−	−	↓
	olfactory habituation/distinguish	−	−	−
Repetitive behavior	grooming	−	−	↑
	rearing	−	−	−
	climbing & jumping	−	−	↑
	marble burying test (digging)	−	−	↓
Language	ultrasonic vocalizations (USVs)	−	−	↓
Learning and memory	novel object recognition	−	−	−
	novel place recognition	−	↓	↓
	Y-maze (reference & spatial memory)	−	↓	↓
	Morris water maze	−	−	−
Motor function	open field test (locomotion)	−	−	−
	rotarod (motor coordination)	−	−	−
Anxiety level	open field test	−	−	−
	elevated zero maze	−	−	−
Pain sensation	hot withdrawal threshold	−	−	−
	mechanical withdrawal threshold	-	-	-

832 **Table S3 Neurodevelopmental reflex outcomes in *Frmd5*-KO mice**

Neurodevelopmental reflex	Genotype		
	WT (N=7)	Het (N=7)	KO (N=7)
Forelimb grasping	3.43±0.20	3.29±0.18	3.43±0.20
Hindlimb grasping	4.43±0.29	4.43±0.20	4.29±0.28
Righting	4.29±0.28	4.14±0.34	4.14±0.26
Cliff avoidance	4.57±0.30	4.86±0.34	4.71±0.29
Hindlimb placing	5.00±0.31	5.14±0.34	4.86±0.26
Gait	7.43±0.30	7.14±0.26	7.14±0.34
Auditory startle	11.43±0.6	11.71±0.28	11.57±0.30
Eye opening	14.43±0.30	14.14±0.27	14.29±0.29
Accelerated righting	15.14±0.26	15.00±0.31	14.86±0.26

833
834

835 **Table S4 Weights and general health outcomes in *Frmd5*-KO mice**

General health	Genotype		
	WT (N=7)	Het (N=7)	KO (N=7)
Body weight (g)			
P1	1.27±0.04	1.30±0.05	1.26±0.04
P3	2.16±0.05	2.21±0.05	2.23±0.03
P7	3.27±0.09	3.36±0.07	3.29±0.04
P14	7.63±0.14	7.66±0.11	7.69±0.05
Adult	24.55±0.41	25.01±0.51	24.8±0.47
Body temperature (℃)	37.23±0.24	37.36±0.15	37.29±0.16
Fur condition (3-point scale)	2	2	2
Skin color (3-point scale)	2	2	2
bald patches (%)	14.29%	14.29%	28.58%
missing whiskers (%)	0%	0%	0%
piloerection (%)	0%	0%	0%

836
837

838 **Table S5 Primary and secondary antibody list**

Antibody	Company	Catalog #	Host Species	Concentration
ACTN1	Proteintech	14788-1-AP	Rabbit	1:1000
ACTN2	HuaAn (HuaBio)	ER1803-60	Rabbit	1:500
AKAP5	ABclonal	A3718	Rabbit	1:1000
CACNG3	Biodragon	BD-PM3400	Rabbit	1:1000
CAMK2A	CST	50049S	Mouse	1:1000
CAMK2B	ABclonal	A2508	Rabbit	1:1000
CAMK2G	Santa Cruz	sc-577278	Mouse	1:200
CAMK4	HuaAn (HuaBio)	ET7107-96	Rabbit	1:1000
CAMKV	Proteintech	14788-1-AP	Rabbit	1:1000
CEP290	Biodragon	BD-PT0859	Rabbit	1:1000
COX4	Abcam	ab110272	Mouse	1:1000
FRMD5	Sigma–Aldrich	HPA013961	Rabbit	1:500
GAPDH	ZSGB-BIO	TA-08	Mouse	1:2000
GFAP	CST	3670s	Mouse	1:1000
GluA1	Abcam	ab109450	Rabbit	1:2000
Histone-H3	Proteintech	17168-1-AP	Rabbit	1:1000
LAMC1	Santa Cruz	sc-374258	Mouse	1:500
MAP2	Rockland	200-901-D68	Chicken	1:1000
NEUN	HuaAn (HuaBio)	ET1602-12	Rabbit	1:1000
NR1	CST	5704s	Rabbit	1:1000
NR2A	CST	4205s	Rabbit	1:1000
NR2B	CST	4207s	Rabbit	1:1000
NR2D	Santa Cruz	sc-17822	Mouse	1:200
PSD95	Abcam	ab18258	Rabbit	1:100-1000
SHANK1	Proteintech	55059-1-AP	Rabbit	1:500
SHANK3	Santa Cruz	sc-377088	Mouse	1:500
SLC6A3	Santa Cruz	sc-32259	Rat	1:500
SMI312	BioLegend	837904	Mouse	1:1000
Synaptophysin	Abcam	ab32127	Rabbit	1:100-1000
anti-Flag-M2	Sigma–Aldrich	F3165	Mouse	1:1000
Donkey anti-Rabbit IgG (H+L), HRP Conjugated	Jackson	715-035-151	Donkey	1:5000-10000
Donkey anti-Mouse IgG (H+L), HRP Conjugated	Jackson	711-035-152	Donkey	1:5000-1000
Goat anti-Rat IgG antibody (H+L), HRP Conjugated	Bioss	bs-0293G-HRP	Goat	1:2000
Goat anti-Chicken IgY (H+L), Alexa Fluor 555	Invitrogen	A-21437	Goat	1:1000
Donkey anti-Mouse IgG (H+L), Alexa Fluor 488	Invitrogen	A-21202	Donkey	1:1000
Donkey anti-Mouse IgG (H+L), Alexa Fluor 594	Invitrogen	A-21203	Donkey	1:1000
Donkey anti-Rabbit IgG (H+L), Alexa Fluor 488	Invitrogen	A-21206	Donkey	1:1000
Donkey anti-Rabbit IgG (H+L), Alexa Fluor 594	Invitrogen	A-21207	Donkey	1:1000
Donkey anti-Rabbit IgG (H+L), Alexa Fluor 647	Invitrogen	A-31573	Donkey	1:1000

839